Dalton Transactions

RSC Publishing

PAPER

View Article Online
View Journal | View Issue

Downloaded by University of Birmingham on 04 January 2013
Published on 31 October 2012 on http://pubs.rsc.org | doi:10.1039/C2DT32160B

Cite this: *Dalton Trans.*, 2013, **42**, 1073

Tuning the photophysical properties of cationic iridium(III) complexes containing cyclometallated 1-(2,4-difluorophenyl)-1*H*-pyrazole through functionalized 2,2′-bipyridine ligands: blue but not blue enough†

Etienne Baranoff,[a,b] Henk J. Bolink,*[c,d] Edwin C. Constable,[e] Manuel Delgado,[c] Daniel Häussinger,[e] Catherine E. Housecroft,*[e] Mohammad K. Nazeeruddin,[a] Markus Neuburger,[e] Enrique Ortí,*[c] Gabriel E. Schneider,[e] Daniel Tordera,[c] Roché M. Walliser[e] and Jennifer A. Zampese[e]

Four new heteroleptic iridium(III) complexes in the family $[Ir(dfppz)_2(N^N)]^+$, where Hdfppz = 1-(2,4-difluorophenyl)-1*H*-pyrazole and N^N = 6-phenyl-2,2′-bipyridine (**1**), 4,4′-(di-*tert*-butyl)-6-phenyl-2,2′-bipyridine (**2**), 4,4′-(di-*tert*-butyl)-6,6′-diphenyl-2,2′-bipyridine (**3**) and 4,4′-bis(dimethylamino)-2,2′-bipyridine (**4**), have been synthesized as the hexafluoridophosphate salts and fully characterized. Single crystal structures of ligand **3** and the precursor $[Ir_2(dfppz)_4(\mu\text{-}Cl)_2]$ have been determined, along with the structures of the complexes $4\{[Ir(dfppz)_2(\mathbf{1})][PF_6]\}\cdot 3CH_2Cl_2$, $[Ir(dfppz)_2(\mathbf{3})][PF_6]\cdot CH_2Cl_2$ and $[Ir(dfppz)_2(\mathbf{4})][PF_6]\cdot CH_2Cl_2$. The role of inter- and intramolecular face-to-face π-stacking in the solid state is discussed. In the $[Ir(dfppz)_2(N^N)]^+$ (N^N = **1–3**) cations, the phenyl substituent in ligands **1**, **2** or **3** undergoes hindered rotation on the NMR timescale at 298 K in solution and the systems have been studied by variable temperature NMR spectroscopy. Acetonitrile solutions of $[Ir(dfppz)_2(N^N)][PF_6]$ (N^N = **1–3**) exhibit similar absorption spectra arising from ligand-based transitions; absorption intensity is enhanced on going to $[Ir(dfppz)_2(\mathbf{4})][PF_6]$ and the spectrum extends further into the visible region. Acetonitrile solutions of the complexes are blue emitters with λ_{em} = 517, 505, 501 and 493 nm for N^N = **1**, **2**, **3** and **4**, respectively (λ_{exc} = 280–310 nm). The redox behaviours of $[Ir(dfppz)_2(N^N)][PF_6]$ (N^N = **1–3**) are similar, and the introduction of the electron-donating NMe_2 substituents onto the N^N ligand shifts the metal-centred oxidation to less positive potentials. Theoretical calculations predict a mixed metal-to-ligand/ligand-to-ligand charge transfer (MLCT/LLCT) character for the emitting triplet state in agreement with the broad and unstructured character of the emission bands. The NMe_2 substituents enlarge the HOMO–LUMO gap and blue-shifts the emission of $[Ir(dfppz)_2(\mathbf{4})]^+$ that is centred on the ancillary ligand. These complexes, when processed into a thin film and sandwiched between two electrodes, lead to very low voltage operating electroluminescent devices. No additional components are needed, which demonstrates their electron and hole transport abilities in conjunction with the luminescent properties.

Received 18th September 2012,
Accepted 16th October 2012

DOI: 10.1039/c2dt32160b

www.rsc.org/dalton

Introduction

Cationic iridium complexes have been extensively used in electroluminescence applications like organic light-emitting diodes (OLEDs) and light-emitting electrochemical cells (LECs).[1,2] The most efficient and stable organic light-emitting devices are based on a multi-stack of small molecular-weight components that use air-sensitive injection layers or metals for efficient electron injection.[3] The multi-layer architecture is obtained by sequentially evaporating the active species under high-vacuum conditions. These devices require rigorous

[a]*EPFL SB ISIC LPI, CH B2 425 (Bâtiment CH), Station 6, CH-1015 Lausanne, Switzerland*
[b]*School of Chemistry, University of Birmingham, Edgbaston, Birmingham, B15 2TT, UK*
[c]*Instituto de Ciencia Molecular, Universidad de Valencia, Catedrático José Beltrán 2, Paterna, E-46980, Spain. E-mail: henk.bolink@uv.es*
[d]*Fundació General de la Universitat de Valencia (FGUV), PO Box 22085, Valencia, Spain*
[e]*Department of Chemistry, University of Basel, Spitalstrasse 51, CH-4056 Basel, Switzerland. E-mail: catherine.housecroft@unibas.ch*

†Electronic supplementary information (ESI) available: Theoretically optimised geometries (Table S1), molecular orbital distribution (Fig. S1) and TD-DFT results (Table S2). CCDC 890056–890060. For ESI and crystallographic data in CIF or other electronic format see DOI: 10.1039/c2dt32160b

Published on 31 October 2012 on http://pubs.rsc.org | doi:10.1039/C2DT32160B
Downloaded by University of Birmingham on 04 January 2013

encapsulation to prevent degradation of the electron-injecting layers. LECs have a much simpler architecture and do not rely on air-sensitive charge-injection layers or metals for electron injection.[4] This greatly simplifies their preparation and makes them more cost efficient. In its simplest form, they consist of a single active layer composed of an ionic transition-metal complex (iTMC).[5–7] The presence of mobile ions facilitates the formation of ionic junctions that lowers the barrier for electron and hole injection and makes these devices independent of the work function of the electrode material.[8,9] Significant advances have been obtained in iTMC-based LECs during the last years.[10–15] This was possible not in the least due to a more thorough understanding of the operation mechanism.[9,14,16–19] Despite these advances, there is one noteworthy deficiency with this type of device, the lack of wide bandgap iTMCs that lead to efficient blue and green iTMC-LECs. Although several blue light-emitting iTMC-based LECs have been reported, their performances are rather poor.[13,20–26] Efficiencies up to 18.3 cd A^{-1} at a luminance of 14.5 cd m^{-2} have been reported by He and co-workers on blue-green LECs by using bulky side groups.[26] With deeper blue emission, the performances are even worse: 2.6 cd A^{-1} for a sky-blue LEC reported by Chen *et al.*[23] and 0.55 cd A^{-1} for the bluest LEC reported so far, by He and co-workers.[20]

In this paper, we report the synthesis and characterization of four iridium(III) complexes of the family $[Ir(dfppz)_2(N^N)]^+$ in which Hdfppz = 1-(2,4-difluorophenyl)-1*H*-pyrazole and N^N are the chelating ligands **1–4** (Scheme 1). Ligands **2–4** contain electron-releasing ^{t}Bu or NMe_2 substituents, introduced to shift the emission maxima of the complexes towards the blue with respect to non-substituted analogues, *e.g.* $[Ir(dfppz)_2(\mathbf{2})]^+$ *versus* $[Ir(dfppz)_2(\mathbf{1})]^+$.

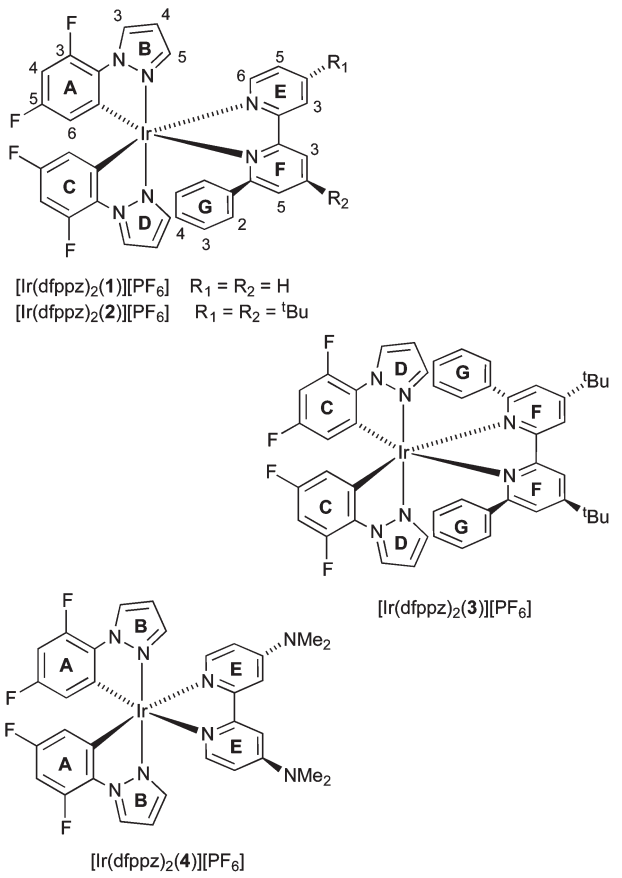

Scheme 1 Ring labelling and atom numbering for NMR spectroscopic assignments.

Experimental

General

^{1}H, ^{13}C and ^{19}F NMR spectra were recorded on Bruker DRX-400, DRX-500, DRX-600 or Bruker Avance III-400, Avance III-500, or Avance III-600 NMR spectrometers; for ^{1}H and ^{13}C NMR spectra, chemical shifts were referenced to residual solvent peaks with respect to δ(TMS) = 0 ppm, and for ^{19}F, an external reference of $CFCl_3$ (δ = 0 ppm) was used. Solution absorption spectra were recorded on an Agilent 8453 spectrophotometer. FT-IR spectra were recorded using a Shimadzu 8400S instrument with Golden Gate accessory for solid samples. Electrospray ionization (ESI) mass spectra were measured using a Bruker esquire 3000^{plus} mass spectrometer. Electrochemical measurements were carried out using cyclic voltammetry and were recorded using a VersaSTAT 3 potentiostat from Princeton Applied Research with glassy carbon working and platinum auxiliary electrodes; a silver wire was used as a pseudo-reference electrode. Solvent was dry, purified MeCN and 0.1 M $[^nBu_4N][PF_6]$ was used as supporting electrolyte. Cp_2Fe was used as internal reference. A Biotage Initiator 8 reactor was used for the syntheses under microwave conditions. Fluka silica 60 and Merck alumina 90 were used for column chromatography. NH_4PF_6 was purchased from Alfa Aesar and used without further purification. $[Ir_2(dfppz)_2(\mu\text{-}Cl)_2]$ was prepared by the method reported by Nonoyama,[27] and ligands **1**,[28] **2**,[29] **3**[30] and **4**[31] by literature procedures.

$[Ir(dfppz)_2(1)][PF_6]$. $[Ir_2(dfppz)_2(\mu\text{-}Cl)_2]$ (70.0 mg, 0.060 mmol) and compound **1** (28.0 mg, 0.121 mmol) were added to MeOH (15 cm^3) in an argon flushed vial. The yellow suspension was heated in a microwave reactor for 2 h (120 °C, 12 bar). The reaction mixture was cooled to room temperature and an excess of solid NH_4PF_6 was added. The mixture was stirred for 1.5 h at room temperature and then evaporated to dryness. The product was purified by column chromatography (silica/CH_2Cl_2 changing to CH_2Cl_2 : MeOH 100 : 3 followed by alumina with the same eluents). $[Ir(dfppz)_2(\mathbf{1})][PF_6]$ was isolated as a yellow solid (79.3 mg, 0.0855 mmol, 71.2%). ^{1}H NMR (600 MHz, CD_2Cl_2, 298 K) δ/ppm 8.52 (dd, J = 8.1, 1.2 Hz, 1H, H^{F3}), 8.45 (d, J = 8.1 Hz, 1H, H^{E3}), 8.36 (d, J = 2.9 Hz, 1H, H^{D3}), 8.30 (t, J = 7.9 Hz, 1H, H^{F4}), 8.24 (d, 1H, H^{B3}), 8.21 (overlapping m, 2H, H^{E6+E5}), 7.60 (dd, J = 7.8, 1.2 Hz, 1H, H^{F5}), 7.52 (ddd, J = 7.5, 5.6, 1.2 Hz, 1H, H^{E4}), 7.26 (d, J = 2.3 Hz, 1H, H^{D5}), 7.13 (t, J = 7.5 Hz, 1H, H^{G4}), 6.96 (br, H^{G3}), 6.78 (t, J = 2.6 Hz, 1H, H^{B5}), 6.62 (m, 1H, H^{A4}), 6.57 (t, J = 2.7 Hz, 1H, H^{B4}), 6.38 (d, J = 2.4 Hz, 1H, H^{B5}), 6.22 (m, 1H, H^{C4}), 5.99 (v br, H^{G2}, but see text), 5.46 (m, 1H, H^{A6}), 4.95 (m, 1H, H^{C6}). ^{13}C NMR: see Table 2. $^{19}F\{^1H\}$ NMR (376 MHz, CD_2Cl_2, 298 K)

This journal is © The Royal Society of Chemistry 2013

Published on 31 October 2012 on http://pubs.rsc.org | doi:10.1039/C2DT32160B
Downloaded by University of Birmingham on 04 January 2013

δ/ppm −74.1 (d, J_{PF} = 711 Hz, $[PF_6]^-$), −112.3 (d, J_{FF} = 6.5 Hz, $F^{C5/A5}$), −115.0 (d, J_{FF} = 6.1 Hz, $F^{C5/A5}$), −124.3 (d, J_{FF} = 6.4 Hz, $F^{C3/A3}$), −125.4 (d, J_{FF} = 6.0 Hz, $F^{C3/A3}$). IR (solid, ν, cm^{-1}): 3164 w, 3084 w, 1617 m, 1608 m, 1577 m, 1560 m, 1510 w, 1478 s, 1450 m, 1445 m, 1420 s, 1338 w, 1309 w, 1259 m, 1253 m, 1230 w, 1182 w, 1167 m, 1122 w, 1110 s, 1074 m, 1039 s, 987 s, 965 w, 917 w, 894 w, 880 w, 839 s, 825 s, 815 s, 780 m, 758 m, 749 s, 737 s, 718 m, 699 m, 645 m, 626 s, 621 m, 610 s. ESI MS: *m*/*z* 783.2 $[M - PF_6]^+$ (calc. 783.2). UV-Vis λ/nm (ε/dm^3 mol^{-1} cm^{-1}) (MeCN, 1.00 × 10^{-5} mol dm^{-3}) 247 (36 100), 307 (17 000). Emission (MeCN, 1.00 × 10^{-5} mol dm^{-3}, λ_{ex} = 307 nm): λ_{em} = 517 nm. Found C 41.09, H 2.36, N 8.13; $C_{34}H_{22}F_{10}IrN_6P{\cdot}CH_2Cl_2$ requires C 41.51, H 2.39, N, 8.30.

[Ir(dfppz)$_2$(2)][PF$_6$]. $[Ir_2(dfppz)_2(\mu\text{-}Cl)_2]$ (70.0 mg, 0.060 mmol) and compound **2** (41.5 mg, 0.121 mmol) were added to MeOH (15 cm^3) in an argon flushed vial, and the yellow suspension was heated in a microwave reactor for 2 h (120 °C, 11 bar). The reaction mixture was cooled to room temperature and solid NH_4PF_6 was added. After 20 h, no precipitation had occurred and so an excess of $AgPF_6$ was added and the mixture stirred for 1 h. Solvent was then removed, and the crude material was purified twice by column chromatography (silica/CH_2Cl_2 changing to CH_2Cl_2 : MeOH 100 : 3 followed by alumina with the same eluents). $[Ir(dfppz)_2(2)][PF_6]$ was isolated as a yellow solid (89.0 mg, 0.0856 mmol, 71.3%). ^{1}H NMR (500 MHz, CD_2Cl_2, 298 K) δ/ppm 8.36 (d, J = 2.8 Hz, 1H, H^{D3}), 8.31 (d, J = 2.0 Hz, 1H, H^{F3}), 8.28 (overlapping, 2H, H^{E3+B3}), 8.07 (d, J = 5.8 Hz, 1H, H^{E6}), 7.53 (d, J = 1.9 Hz, 1H, H^{F5}), 7.48 (m, 1H, H^{E5}), 7.24 (d, J = 2.1 Hz, 1H, H^{D5}), 7.14 (t, J = 7.5 Hz, 1H, H^{G4}), 6.95 (br, 2H, H^{G3}), 6.77 (t, J = 2.6 Hz, 1H, H^{D4}), 6.61 (m, 1H, H^{A4}), 6.59 (t, J = 2.8 Hz, 1H, H^{B4}), 6.37 (d, J = 2.5 Hz, 1H, H^{B5}), 6.21 (m, 1H, H^{C4}), 6.03 (v br, H^{G2}, but see text), 5.47 (m, 1H, H^{A6}), 4.93 (m, 1H, H^{C6}), 1.51 (s, 9H, $H^{Me,\ ring\ F}$), 1.45 (s, 9H, $H^{Me,\ ring\ E}$). ^{13}C NMR: see Table 2. $^{19}F\{^1H\}$ NMR (376 MHz, CD_2Cl_2, 298 K) δ/ppm −74.2 (d, J_{PF} = 711 Hz, $[PF_6]^-$), −112.4 (d, J_{FF} = 6.2 Hz, $F^{C5/A5}$), −115.1 (d, J_{FF} = 5.9 Hz, $F^{C5/A5}$), −124.5 (d, J_{FF} = 6.2 Hz, $F^{C3/A3}$), −125.5 (d, J_{FF} = 5.9 Hz, $F^{C3/A3}$). IR (solid, ν, cm^{-1}): 3177 w, 2956 w, 1611 m, 1580 m, 1542 w, 1480 s, 1438 w, 1419 s, 1369 w, 1337 w, 1309 w, 1251 m, 1166 w, 1125 w, 1106 m, 1073 m, 1037 s, 987 s, 963 w, 908 w, 825 s, 804 s, 771 m, 752 m, 743 s, 703 s, 655 w, 625 m, 602 s. ESI MS *m*/*z*: 895.4 $[M - PF_6]^+$ (calc. 895.3). UV-Vis λ/nm (ε/dm^3 mol^{-1} cm^{-1}) (MeCN, 1.00 × 10^{-5} mol dm^{-3}): 218 sh (57 500), 250 (42 000), 309 (19 900). Emission (MeCN, 1.00 × 10^{-5} mol dm^{-3}, λ_{ex} = 305 nm): λ_{em} = 505 nm. Found C 46.51, H 3.63, N 7.64; $C_{42}H_{38}F_{10}IrN_6P{\cdot}0.75CH_2Cl_2$ requires C 46.52, H 3.61, N, 7.61.

[Ir(dfppz)$_2$(3)][PF$_6$]. $[Ir_2(dfppz)_2(\mu\text{-}Cl)_2]$ (100.0 mg, 0.0853 mmol), **3** (75.3 mg, 0.179 mmol) and $AgPF_6$ (45.3 mg, 0.179 mmol) were combined with MeOH (15 cm^3) in an argon flushed vial. This was placed in a microwave reactor for 2 h at 120 °C (P = 13 bar). The vial was removed from the reactor and CH_2Cl_2 (3 cm^3) was added. The reaction mixture was heated for further 15 min at 100 °C (P = 11 bar) in the microwave reactor. The yellow-green solution was cooled to room temperature and an excess of solid NH_4PF_6 was added. The mixture was stirred for 1 h at room temperature and then evaporated to dryness. The product was purified by chromatography (column, alumina with CH_2Cl_2 changing to CH_2Cl_2 : MeOH 100 : 5, then preparative TLC, alumina, CH_2Cl_2 : MeOH 100 : 1.5). $[Ir(dfppz)_2(3)][PF_6]$ was isolated as a yellow solid (99.6 mg, 0.089 mmol, 52.3%). ^{1}H NMR (500 MHz, CD_2Cl_2, 298 K) δ/ppm 8.32 (d, J = 2.1 Hz, 2H, H^{F3}), 8.19 (d, J = 2.9 Hz, 2H, H^{D3}), 7.38 (d, J = 2.0 Hz, 2H, H^{F5}), 7.14 (overlapping m, 4H, H^{G4+D5}), 6.94 (br, 4H, H^{G3}), 6.70 (t, J = 2.6 Hz, 2H, H^{D4}), 6.64 (v br., H^{G2}), 6.16 (m, 2H, H^{C4}), 4.47 (m, 2H, H^{C6}), 1.48 (s, 18H, H^{Me}). ^{13}C NMR: see Table 2. $^{19}F\{^1H\}$ NMR (376 MHz, CD_2Cl_2, 298 K) δ/ppm −73.7 (d, J_{PF} = 711 Hz, $[PF_6]^-$), −113.7 (d, J_{FF} = 5.9 Hz, F^{C5}), −125.5 (d, J_{FF} = 5.9 Hz, F^{C3}). IR (solid, ν, cm^{-1}): 3152 w, 3091 w, 2968 w, 2874 w, 1613 m, 1584 m, 1544 w, 1500 w, 1480 m, 1440 w, 1419 m, 1398 m, 1369 w, 1338 w, 1307 w, 1251 m, 1215 w, 1166 w, 1125 w, 1105 m, 1070 m, 1037 m, 986 s, 961 w, 914 w, 880 w, 829 s, 819 s, 801 m, 754 s, 697 s, 662 w, 626 m. ESI-MS *m*/*z* 971.5 $[M - PF_6]^+$ (calc. 971.3). UV-Vis λ/nm (ε/dm^3 mol^{-1} cm^{-1}) (MeCN, 1.00 × 10^{-5} mol dm^{-3}): 235 (45 900), 274 (27 300), 306 (16 850), 318sh (15 000). Emission (MeCN, 1.00 × 10^{-5} mol dm^{-3}, λ_{ex} = 310 nm): λ_{em} = 501 nm. Found C 51.57, H 3.93, N 7.55; $C_{42}H_{38}F_{10}IrN_6P{\cdot}0.25CH_3OH$ requires C 51.56, H 3.86, N, 7.48.

[Ir(dfppz)$_2$(4)][PF$_6$]. $[Ir_2(dfppz)_2(\mu\text{-}Cl)_2]$ (70.0 mg, 0.060 mmol) and compound **4** (29.2 mg, 0.121 mmol) were added to MeOH (15 cm^3) in an argon flushed vial, and this was heated in a microwave reactor for 2 h (120 °C, 11 bar). The yellow solution was cooled to room temperature and an excess of solid NH_4PF_6 was added. The mixture was stirred for 1.5 h at room temperature and then evaporated to dryness. The crude material was purified by column chromatography (silica/CH_2Cl_2 changing to CH_2Cl_2 : MeOH 100 : 3 followed by alumina with the same eluents). $[Ir(dfppz)_2(4)][PF_6]$ was isolated as a yellow-green solid (50.5 mg, 0.0539 mmol, 44.8%). ^{1}H NMR (500 MHz, CD_2Cl_2) δ/ppm 8.36 (d, J = 2.8 Hz, 2H, H^{B3}), 7.53 (d, J = 6.7 Hz, 2H, H^{E6}), 7.30 (d, J = 2.6 Hz, 2H, H^{E3}), 6.93 (d, J = 2.1 Hz, 2H, H^{B5}), 6.67 (m, 2H, H^{A4}), 6.59 (t, J = 2.6 Hz, 2H, H^{B4}), 6.49 (dd, J = 6.7, 2.6 Hz, 2H, H^{E5}), 5.78 (m, 2H, H^{A6}), 3.19 (s, 12H, CH_3). ^{13}C NMR: see Table 2. $^{19}F\{^1H\}$ NMR (376 MHz, CD_2Cl_2, 298 K) δ/ppm −74.1 (d, J_{PF} = 711 Hz, $[PF_6]^-$), −114.2 (d, J_{FF} = 5.9 Hz, F^{A5}), −125.3 (d, J_{FF} = 5.5 Hz, F^{A3}). IR (solid, ν, cm^{-1}): 3166 w, 2928 w, 1612 s, 1585 m, 1576 m, 1544 m, 1512 w, 1474 m, 1434 m, 1420 m, 1380 m, 1337 w, 1309 w, 1285 m, 1253 m, 1226 w, 1187 w, 1165 w, 1108 m, 1072 m, 1034 s, 1016 m, 987 s, 962 w, 916 w, 834 s, 825 s, 808 s, 803 s, 746 m, 740 m, 710 w, 655 w, 626 m, 602 s. ESI MS *m*/*z*: 971.5 $[M - PF_6]^+$ (calc. 971.3). UV-Vis λ/nm (ε/dm^3 mol^{-1} cm^{-1}) (MeCN, 1.00 × 10^{-5} mol dm^{-3}): 216 sh (48 800), 260 (42 000), 352 (8600). Emission (MeCN, 1.00 × 10^{-5} mol dm^{-3}, λ_{ex} = 280 nm): λ_{em} = 493 nm. Found C 39.24, H 2.86, N 11.28; $C_{42}H_{38}F_{10}IrN_6P{\cdot}0.75CH_2Cl_2$ requires C 39.28, H 2.97, N, 11.19.

Crystallography

Data were collected on either a Bruker-Nonius KappaAPEX diffractometer with data reduction, solution and refinement

Published on 31 October 2012 on http://pubs.rsc.org | doi:10.1039/C2DT32160B
Downloaded by University of Birmingham on 04 January 2013

Table 1 Crystallographic data for ligand **3** and the complexes $[Ir_2(dfppz)_2(\mu\text{-}Cl)_2]\cdot CH_2Cl_2$, 4{$[Ir(dfppz)_2(\mathbf{1})][PF_6]\}\cdot 3CH_2Cl_2$, $[Ir(dfppz)_2(\mathbf{3})][PF_6]\cdot CH_2Cl_2$ and $[Ir(dfppz)_2(\mathbf{4})][PF_6]\cdot CH_2Cl_2$

Compound	**3**	$[Ir_2(dfppz)_2(\mu\text{-}Cl)_2]\cdot CH_2Cl_2$	4{$[Ir(dfppz)_2(\mathbf{1})]$-$[PF_6]\}\cdot 3CH_2Cl_2$	$[Ir(dfppz)_2(\mathbf{3})]$-$[PF_6]\cdot CH_2Cl_2$	$[Ir(dfppz)_2(\mathbf{4})]$-$[PF_6]\cdot CH_2Cl_2$
Formula	$C_{30}H_{32}N_2$	$C_{37}H_{22}Cl_4F_8Ir_2N_8$	$C_{139}H_{94}Cl_6F_{40}Ir_4N_{24}P_4$	$C_{49}H_{44}Cl_2F_{10}IrN_6P$	$C_{33}H_{30}Cl_2F_{10}IrN_8P$
Formula weight	420.60	1256.87	3965.84	1200.99	1022.74
Crystal colour and habit	Colourless needle	Yellow block	Yellow block	Yellow block	Yellow block
Crystal system	Monoclinic	Triclinic	Monoclinic	Monoclinic	Triclinic
Space group	*C*2/*c*	$P\bar{1}$	$P2_1/n$	$P2_1/c$	$P\bar{1}$
a, *b*, *c*/Å	19.8624(12)	10.753(3)	16.662(5)	20.8613(17)	9.5146(9)
	6.1354(3)	12.323(4)	10.561(3)	10.0629(5)	14.3727(12)
	19.9421(13)	16.058(4)	19.725(6)	25.126(2)	14.4945(14)
α, β, γ/°	90	80.37(2)	90	90	102.341(7)
	106.045(5)	84.700(19)	92.00(3)	114.381(6)	102.295(8)
	90	65.47(2)	90	90	105.066(7)
U/Å^3	2335.6(2)	1907.9(9)	3468.9(18)	4804.2(6)	1792.4(3)
*D*c/Mg m^{-3}	1.196	2.188	1.898	1.660	1.895
Z	4	2	1	4	2
μ (Mo-Kα)/mm^{-1}	0.069	7.329	4.102	3.005	4.010
T/K	123	173	173	173	173
Refln. collected (R_{int})	87 729 (0.052)	20 996 (0.0755)	54 439 (0.0696)	33 704 (0.2023)	39 217 (0.1096)
Unique refln.	6278	8332	7625	8485	6484
Refln. for refinement	5840	7239	6628	6560	6436
Parameters	145	532	497	628	646
Threshold	$I > 2.0\sigma$	$I > 2.0\sigma$	$I > 2.0\sigma$	$I > 2.0\sigma$	$I > 2.0\sigma$
R_1 (R_1 all data)	0.0517 (0.0560)	0.0399 (0.0476)	0.0581 (0.0668)	0.0876 (0.1085)	0.0436 (0.0438)
wR_2 (wR_2 all data)	0.0552 (0.0552)	0.0980 (0.1018)	0.1481 (0.1545)	0.2121 (0.2294)	0.1171 (0.1173)
Goodness of fit	1.0471	1.098	1.096	1.067	1.181
CCDC deposition	890 060	890 057	890 056	890 058	890 059

using the programs APEX2,[32] SIR92[33] and CRYSTALS,[34] or on a Stoe IPDS diffractometer using Stoe IPDS[35] software and SHELXL97.[36] The program ORTEP-3 for Windows was used to draw the ORTEP diagrams,[37] and structures were analysed using Mercury v. 2.4.[38,39] Crystallographic data are listed in Table 1.

Photophysics

The photoluminescence spectra and quantum yields of $[Ir(dfppz)_2(N\hat{}N)][PF_6]$ complexes (N^N = **1–4**) in 90 nm thin films of 5% in weight of the complexes mixed with 95% in weight of PMMA and the complexes mixed with the ionic liquid 1-butyl-3-methylimidazolium hexafluoridophosphate (>98.5%, Sigma-Aldrich) in a 4 to 1 molar ratio were measured with a Hamamatsu C9920-02 Absolute PL Quantum Yield Measurement System (λ_{exc} = 310 nm).

Computational details

Density functional calculations (DFT) were carried out with the C.01 revision of the Gaussian 09 program package[40] using Becke's three-parameter B3LYP exchange-correlation functional[41,42] together with the 6-31G** basis set for C, H, F, and N,[43] and the "double-ζ" quality LANL2DZ basis set for Ir.[44] The geometries of the singlet ground state and of the lowest-energy triplet state were fully optimized without imposing any symmetry restriction. The geometry of the first triplet state was calculated at the spin-unrestricted UB3LYP level with a spin multiplicity of 3. All the calculations were performed in the presence of solvent (acetonitrile). Solvent effects were considered within the self-consistent reaction field (SCRF) theory using the SMD keyword that performs a polarized continuum model (PCM)[45–47] calculation using the solvation model of Thrular *et al.*[48] The SMD solvation model is based on the polarized continuous quantum chemical charge density of the solute (the "D" in the name stands for "density"). Time-dependent DFT (TD-DFT) calculations of the lowest-lying 20 triplets were performed in the presence of the solvent at the minimum-energy geometry optimized for the ground state.

Electroluminescent devices

The solvents were supplied by Aldrich. The thickness of films was determined with an Ambios XP-1 profilometer. Indium tin oxide (ITO)-coated glass plates (15 Ω $\square^{-1}$) were patterned by conventional photolithography (Naranjo Substrates). The substrates were cleaned by sonication in water–soap, water and 2-propanol baths, in that order. After drying, the substrates were placed in a UV-ozone cleaner (Jelight 42-220) for 20 min.

The electroluminescent devices were made as follows. First, a 90 nm layer of poly-(3,4-ethylenedioxythiophene) : poly-(styrenesulfonate) (PEDOT : PSS, CLEVIOS™ P VP AI 4083, aqueous dispersion, 1.3–1.7% solid content, Heraeus) was spin-coated onto the ITO glass substrate to improve the reproducibility of the devices and to prevent the formation of pinholes. Then, 90 nm transparent films of $[Ir(dfppz)_2(N\hat{}N)][PF_6]$ complexes (N^N = **1–4**) and the ionic liquid 1-butyl-3-methylimidazolium hexafluoridophosphate (>98.5%, Sigma-Aldrich) in a 4 to 1 molar ratio were spin-coated from 20 mg cm^{-3} acetonitrile solution at 1000 rpm for 20 s. The device was transferred into an inert atmosphere glovebox (<0.1 ppm O_2 and H_2O, M. Braun) and dried on a hot plate at 100 °C for 1 h. The Al electrode (70 nm) was thermally vapor-deposited using

 This journal is © The Royal Society of Chemistry 2013

Downloaded by University of Birmingham on 04 January 2013
Published on 31 October 2012 on http://pubs.rsc.org | doi:10.1039/C2DT32160B

Table 2 ^{13}C NMR spectroscopic data (126 MHz) for the precursor dimer and the four complexes, assigned using low temperature HMQC and HMBC spectra. See Scheme 1 for atom labelling. Coupling constants are in Hz

Compound	A1	A2	A3	A4	A5	A6	B3	B4	B5	C1	C2	C3	C4	C5	C6	D3	D4	D5
$[Ir_2(dfppz)_4Cl_2]$	115.0	128.0	149.2	98.8	159.5	115.1	132.3	107.9	140.7									
			J_{CF} 256		J_{CF} 249													
$[Ir(dfppz)_2(\mathbf{1})][PF_6]$	132.8/136.7[a]	126.5	148.3	99.7	160.0	114.1	131.7	108.9	137.4	132.8/136.7	126.0	147.9	98.0	159.1	114.3	131.4	108.9	138.3
			J_{CF} 256		J_{CF} 256							J_{CF} 256		J_{CF} 260				
$[Ir(dfppz)_2(\mathbf{2})][PF_6]$	134.2/138.1[a]	127.4	149.4	100.3	160.8	114.8	132.3	109.8	138.5	134.2/138.1	127.0	149.0	98.7	160.1	115.2	132.3	109.7	139.0
			J_{CF} 254		J_{CF} 248							J_{CF} 251		J_{CF} 245				
$[Ir(dfppz)_2(\mathbf{3})][PF_6]$										133.7[a]	124.9	147.2	98.2	158.5	113.6	131.7	108.7	138.9
												J_{CF} 254		J_{CF} 252				
$[Ir(dfppz)_2(\mathbf{4})][PF_6]$	139.2[a]	128.0	148.0	99.1	160.8	115.8	131.8	108.9	138.1									
			J_{CF} 242		J_{CF} 228													
	E2	E3	E4	E5	E6	F2	F3	F4	F5	F6	G1	G2/G6	G3/G5	G4	Me	C^4Bu		
$[Ir(dfppz)_2(\mathbf{1})][PF_6]$	157.2	124.9	127.5	140.0	150.1	164.2	122.7	140.2	129.1	165.6	137.8	126.9/127.3	127.2/128.0	129.3				
$[Ir(dfppz)_2(\mathbf{2})][PF_6]$	157.7	122.4	165.7	125.8	150.5	158.3	120.4	165.9	127.2	166.3	139.1	128.0/128.5	128.0/129.0	130.2	30.8	36.45		
															30.7	36.40		
$[Ir(dfppz)_2(\mathbf{3})][PF_6]$						157.9	120.6	163.9	127.0	164.4	138.2	126.6/127.3	127.3/127.4	128.5	30.0	35.7		
$[Ir(dfppz)_2(\mathbf{4})][PF_6]$	149.3	105.9	156.3	109.4	149.8										40.0			

[a] For $[Ir(dfppz)_2(N^N)][PF_6]$ (N^N = **1–4**), signal for C^{A1} only resolved in 151 MHz ^{13}C NMR spectra (298 K).

a shadow mask under a vacuum (<1 × 10^{-6} mbar) with an Edwards Auto500 evaporator integrated into the inert atmosphere glovebox. The area of the device was 6.534 mm^2. The devices were not encapsulated and were characterized inside the glovebox at room temperature. Device lifetime was measured by applying pulsed currents and monitoring the voltage and luminance by a True Colour Sensor MAZeT (MTCSiCT Sensor) with a Botest OLT OLED Lifetime-Test System.

Results and discussion

Preparation of complexes and their mass spectrometric and solution NMR spectroscopic characterization

The complexes $[Ir(dfppz)_2(N^N)][PF_6]$ (N^N = **1–4**) were prepared by the established methodology[49] of treating a $[Ir(C^N)_2(\mu\text{-}Cl)_2]$ dimer with two equivalents of an N^N ligand (Scheme 2). Yields ranged from 45% for $[Ir(dfppz)_2(\mathbf{4})][PF_6]$ to 71% for $[Ir(dfppz)_2(\mathbf{1})][PF_6]$ and $[Ir(dfppz)_2(\mathbf{2})][PF_6]$. The ESI mass spectrum of each complex was assigned to the $[M - PF_6]^+$ ion, and the observed isotope patterns were in accord with those simulated.

Although the dimer $[Ir_2(dfppz)_4(\mu\text{-}Cl)_2]$ (Scheme 2) has been used as a synthon on numerous occasions,[11,26,30,50–57] assignment of the solution ^{13}C NMR spectrum appears to be missing from the literature. Since this provides a good starting point for the assignment of the NMR spectra of the $[Ir(dfppz)_2(N^N)][PF_6]$ complexes, we include the data in Table 2. The ^1H and

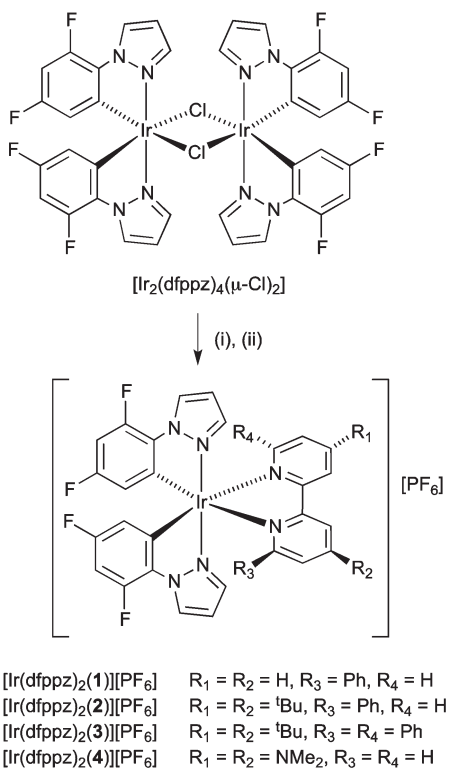

Scheme 2 Syntheses of the complexes described in this work. Conditions: (i) Ligand **1**, **2**, **3** or **4**, MeOH, microwave, 2 h; (ii) $[NH_4][PF_6]$.

Published on 31 October 2012 on http://pubs.rsc.org | doi:10.1039/C2DT32160B
Downloaded by University of Birmingham on 04 January 2013

^{13}C NMR spectra of $[Ir_2(dfppz)_4(\mu\text{-}Cl)_2]$ and $[Ir(dfppz)_2(N^\wedge N)][PF_6]$ (N^N = **1–4**) were assigned using routine 2D techniques; COSY, HMQC, HMBC and NOESY spectra for the latter four complexes were recorded at 210 K. Each of $[Ir_2(dfppz)_4(\mu\text{-}Cl)_2]$, $[Ir(dfppz)_2(\mathbf{3})]^+$ and $[Ir(dfppz)_2(\mathbf{4})]^+$ contains a C_2 axis and, therefore, the two cyclometallated ligands are equivalent. In contrast, the two C^N ligands in $[Ir(dfppz)_2(\mathbf{1})]^+$ and $[Ir(dfppz)_2(\mathbf{2})]^+$ are non-equivalent. The ring labelling scheme shown in Scheme 1 has been adopted to allow easy comparison of the spectroscopic data. The ^{13}C NMR spectroscopic data in Table 2 reveal correlations between the chemical shifts for a given ^{13}C nucleus (*e.g.* C^{A4} or C^{B4}) across a set of related complexes. The ^{13}C NMR resonance for the cyclometallated carbon atom (C^{A1}) was observed at δ 115.0 ppm for $[Ir_2(dfppz)_4(\mu\text{-}Cl)_2]$ and was assigned from the weak cross peak in the HMBC spectrum to proton H^{A4}. On going from the chlorido dimer (in which C^{A1} lies *trans* to chlorine) to each of the $[Ir(dfppz)_2(N^\wedge N)][PF_6]$ complexes (C^{A1} lies *trans* to nitrogen), the signal for C^{A1} shifts to higher frequency (Table 2). For complexes in which the two $[dfppz]^-$ ligands are non-equivalent, NOESY cross peaks between the signals for pairs of protons H^{A6}/H^{E6}, H^{A6}/H^{D5} and H^{C6}/H^{B5} allowed rings A and C, and B and D to be distinguished.

In $[Ir(dfppz)_2(N^\wedge N)][PF_6]$ (N^N = **1–3**), each phenyl substituent in ligands **1**, **2** or **3** undergoes hindered rotation on the NMR timescale at 298 K. At 210 K, the 500 MHz ^{1}H NMR spectrum of a CD_2Cl_2 solution of $[Ir(dfppz)_2(\mathbf{1})][PF_6]$ shows signals at δ 7.14 and 5.85 ppm (d, J = 7.6 Hz) assigned to $H^{G2/G6}$ and at δ 7.12 and 6.79 ppm arising from $H^{G3/G5}$. Upon warming, the signals start to collapse, and at 298 K, coalescence of the $H^{G3/G5}$ protons begins giving rise to a broad signal (FWHM ≈ 200 Hz) centred at δ 6.96 ppm; because of the large chemical shift difference between the signals for H^{G2} and H^{G6}, coalescence is not observed at 298 K and the very broad peak centred at δ 6.0 ppm arises from the continuing collapse of one of the $H^{G2/G6}$ signals. On going from $[Ir(dfppz)_2(\mathbf{1})][PF_6]$ to $[Ir(dfppz)_2(\mathbf{2})][PF_6]$, the introduction of the ^{t}Bu substituents (Scheme 2) has little effect on the dynamic process. This is consistent with the ^{t}Bu groups being on the periphery of the complex and having no steric influence on the rotation of phenyl ring G. At 240 K, the 500 MHz ^{1}H NMR spectrum of $[Ir(dfppz)_2(\mathbf{2})][PF_6]$ (in CD_2Cl_2) exhibits signals at δ 7.14 and 5.88 ppm arising from $H^{G2/G6}$ and δ 7.05 and 6.79 ppm due to $H^{G3/G5}$. Coalescence of the latter resonances occurs around 290 K and a broad signal centred at δ 6.95 ppm is observed. As in the room temperature spectrum of $[Ir(dfppz)_2(\mathbf{1})][PF_6]$, a broad signal at δ 6.0 ppm in the spectrum of $[Ir(dfppz)_2(\mathbf{2})][PF_6]$ is due to the continuing collapse of one of the $H^{G2/G6}$ signals. From these coalescence phenomena, it was possible to determine the Gibbs activation enthalpy for the rotation of the phenyl ring *G* using the Eyring equation. $\Delta G^\ddagger$ was calculated to be 53.9 kJ mol^{-1}. For compound $[Ir(dfppz)_2(\mathbf{3})][PF_6]$, a qualitatively similar hindered rotation of the *G* rings was observed. At 298 K, broad signals at δ 6.94 and 6.64 ppm arise from the coalescence of signals for pairs of resonances for $H^{G3/G5}$ and $H^{G2/G6}$ which are observed, respectively, at δ 7.08 and 6.75 ppm and δ 7.05 and 6.03 ppm at 210 K (Fig. 1). From these data $\Delta G^\ddagger$ could be determined to be 60.1 kJ mol^{-1}. A comparison of the Gibbs activation enthalpies of $[Ir(dfppz)_2(\mathbf{2})][PF_6]$ and $[Ir(dfppz)_2(\mathbf{3})][PF_6]$ indicates that the barrier to rotation of the two phenyl rings in $[Ir(dfppz)_2(\mathbf{3})][PF_6]$ is considerably lower than that of the one phenyl substituent in $[Ir(dfppz)_2(\mathbf{2})][PF_6]$.

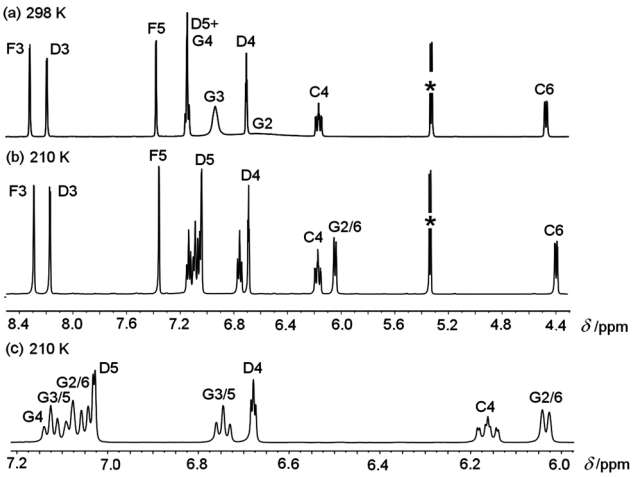

Fig. 1 500 MHz NMR spectra of $[Ir(dfppz)_2(\mathbf{3})][PF_6]$ at (a) 298 K and (b) 210 K. The signal (δ 1.43 ppm) for the ^{t}Bu groups is not shown. Signals * = residual CH_2Cl_2 and $CDHCl_2$. (c) Expansion of part of the spectrum shown in part (b) showing the ring G proton signals.

The $^{19}F\{^1H\}$ NMR spectrum of a CD_2Cl_2 solution of $[Ir(dfppz)_2(\mathbf{3})][PF_6]$ exhibited two doublets (δ −113.7 and −125.5 ppm, J_{FF} = 5.9 Hz) in addition to a doublet at δ −73.7 ppm assigned to the $[PF_6]^-$ ion (J_{PF} = 711 Hz). A similar set of signals was observed for $[Ir(dfppz)_2(\mathbf{4})][PF_6]$. On going to the proton coupled ^{19}F NMR spectrum, the signals at around δ −125 and −114 ppm appeared as a doublet of doublets, and triplet of doublets, respectively, allowing the lower frequency signal to be assigned to F^{A3} (F^{C3} in $[Ir(dfppz)_2(\mathbf{3})][PF_6]$) and the higher frequency signal to F^{A5} (F^{C5} in $[Ir(dfppz)_2(\mathbf{3})][PF_6]$); values of J_{HF} were close to 12 Hz. For each of $[Ir(dfppz)_2(\mathbf{1})][PF_6]$ and $[Ir(dfppz)_2(\mathbf{2})][PF_6]$, the $^{19}F\{^1H\}$ NMR spectrum showed four doublets, in addition to the doublet for the $[PF_6]^-$ ion. Assignments (see Experimental section) were again made based on the changes on going from the $^{19}F\{^1H\}$ to ^{19}F NMR spectra.

Solid-state structures

Despite the popularity of the route illustrated in Scheme 2 for the synthesis of $[Ir(C^\wedge N)_2(N^\wedge N)]^+$ complexes, a search of the Cambridge Structural Database (CSD, v. 5.33 updates May 2012 using Conquest 1.14[38,39]) revealed only twelve structurally characterized dimers of type $[Ir_2(C^\wedge N)_4(\mu\text{-}Cl)_2]$.[58–68] Of these, only the structure of $[Ir_2(dfppy)_4(\mu\text{-}Cl)_2]$[68] (Hdfppy = 2-(2,4-difluorophenyl)pyridine) is related to that of $[Ir(dfppz)_2(\mu\text{-}Cl)_2]$. Single crystals of the latter grew on leaving a CH_2Cl_2 solution of the complex standing at room temperature. The complex crystallizes as $[Ir(dfppz)_2(\mu\text{-}Cl)_2]\cdot CH_2Cl_2$ in the centrosymmetric space group $P\bar{1}$ with both the Λ,Λ- and Δ,Δ-forms of

 This journal is © The Royal Society of Chemistry 2013

Published on 31 October 2012 on http://pubs.rsc.org | doi:10.1039/C2DT32160B
Downloaded by University of Birmingham on 04 January 2013

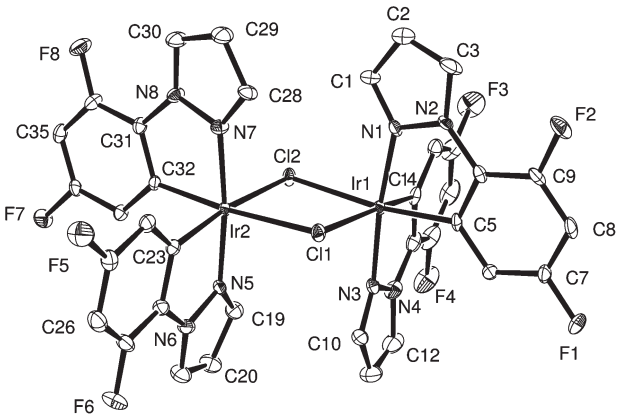

Fig. 2 Structure of Λ,Λ-[Ir(dfppz)$_2$(μ-Cl)$_2$] in [Ir(dfppz)$_2$(μ-Cl)$_2$]·CH_2Cl_2 with ellipsoids plotted at 30% probability level; H atoms omitted. Selected bond parameters: Ir1–C14 = 1.982(6), Ir1–C5 = 1.999(5), Ir1–N1 = 2.028(5), Ir1–N3 = 2.032(5), Ir1–Cl2 = 2.4870(15), Ir1–Cl1 = 2.4962(17), Ir2–C32 = 1.989(5), Ir2–C23 = 2.000(6), Ir2–N5 = 2.014(5), Ir2–N7 = 2.022(5), Ir2–Cl2 = 2.4856(17), Ir2–Cl1 = 2.4951(15) Å; C5–Ir1–N1 = 80.5(2), C14–Ir1–N3 = 80.7(3), Cl2–Ir1–Cl1 = 83.39(5), Cl2–Ir2–Cl1 = 83.45(5), C23–Ir2–N5 = 80.8(2), C32–Ir2–N7 = 80.6(2)°.

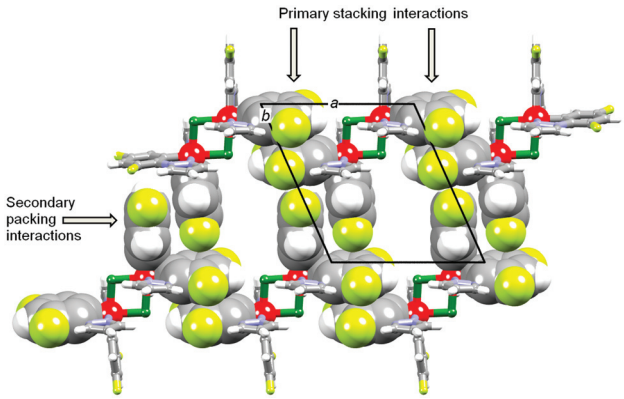

Fig. 3 Assembly of ribbons consisting of Λ,Λ-[Ir(dfppz)$_2$(μ-Cl)$_2$] molecules (each ribbon runs parallel to the *a*-axis) and interdigitation of chains to give sheets in the *ab*-plane.

the dimer in the unit cell. An analogous racemate has been observed in the solid state for [Ir_2(dfppy)$_4$(μ-Cl)$_2$].[68] Fig. 2 depicts the molecular structure of Λ,Λ-[Ir(dfppz)$_2$(μ-Cl)$_2$] present in the asymmetric unit. The structure is unexceptional, exhibiting a *trans*-arrangement of the N-donors of the two cyclometallating ligands. The two Ir atoms are crystallographically independent and bond parameters in the iridium coordination sphere are given in the caption to Fig. 1. Face-to-face π-stacking of pairs of difluorophenyl rings plays a major role in crystal packing. The planes of the rings containing atoms C5 and C32^{i} (symmetry code i = 1 + *x*, *y*, *z*) subtend an angle of 2.6° and the inter-centroid separation is 3.68 Å, leading to an efficient interaction (Fig. 3, primary stacking interaction). These contacts result in the assembly of ribbons that run along the *a*-axis. The chains are interdigitated by virtue of a second set of face-to-face π-stacking interactions, but these are less effective than the interactions that support each chain. The former (labelled secondary stacking interactions in Fig. 3) involve the difluorophenyl rings containing atoms C14 and C23^{ii} (symmetry code ii = −1 + *x*, 1 + *y*, *z*); the angle between the least squares planes of these rings is 8.2°, and the inter-centroid distance is 4.26 Å. This separation is at the extreme of the range discussed by Janiak for similar stacking interactions.[69] The CH_2Cl_2 molecules in [Ir(dfppz)$_2$-(μ-Cl)$_2$]·CH_2Cl_2 are ordered, and participate in CH···π and CCl···π contacts. The only significant packing interactions involving the pyrazole rings are intermolecular CH···F contacts.

X-Ray quality crystals of 4{[Ir(dfppz)$_2$(**1**)][PF_6]}·3CH_2Cl_2 were grown from a CH_2Cl_2 solution of the complex, and the structure of the [Ir(dfppz)$_2$(**1**)]$^+$ cation is depicted in Fig. 4. The complex crystallizes in the centrosymmetric $P2_1/n$ space group with both enantiomers of [Ir(dfppz)$_2$(**1**)]$^+$ in the unit cell. Atom Ir1 is in an octahedral environment, parameters for which are given in the caption to Fig. 4. In keeping with expectations, a

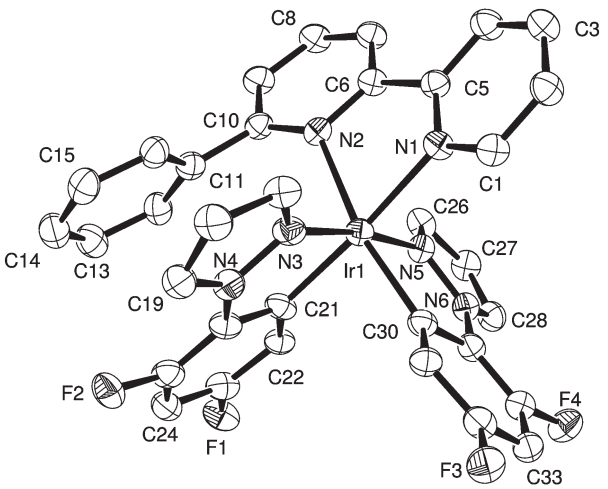

Fig. 4 Structure of the [Ir(dfppz)$_2$(**1**)]$^+$ cation in 4{[Ir(dfppz)$_2$(**1**)][PF_6]}·3CH_2Cl_2 with ellipsoids plotted at 30% probability level; H atoms omitted. Selected bond parameters: Ir1–N3 = 2.021(7), Ir1–N5 = 2.022(6), Ir1–C30 = 2.031(8), Ir1–C21 = 2.035(8), Ir1–N1 = 2.140(7), Ir1–N2 = 2.191(6), N3–N4 = 1.375(10), N5–N6 = 1.357(9) Å; N1–Ir1–N2 = 76.1(2), N3–Ir1–C21 = 79.6(3), N5–Ir1–C30 = 80.2(3)°.

trans-arrangement of the N-donors of the two cyclometallating ligands is observed, and each N-donor of ligand **1** is therefore *trans* to a C-donor of a [dfppz]$^-$ ligand. Whereas the two co-ordinated [dfppz]$^-$ ligands are essentially planar, the bpy domain of **1** deviates significantly from planarity (angle between the least squares planes of the two pyridine rings = 19.5°). It is tempting to state that the origin of the latter is the intra-cation π-stacking interaction described below, and we comment upon this further in the discussion of the structure of [Ir(dfppz)$_2$(**4**)][PF_6]·CH_2Cl_2. The phenyl substituent of ligand **1** is twisted through 57.0° with respect to the pyridine ring to which it is bonded, thereby allowing the phenyl ring to engage in a face-to-face π–π interaction with the difluorophenyl ring of one of the [dfppz]$^-$ ligands. This is shown in a space-filling representation in Fig. 5. In Fig. 4, the π-stacked rings are those containing atoms C11 and C21; the rings are mutually offset

Published on 31 October 2012 on http://pubs.rsc.org | doi:10.1039/C2DT32160B
Downloaded by University of Birmingham on 04 January 2013

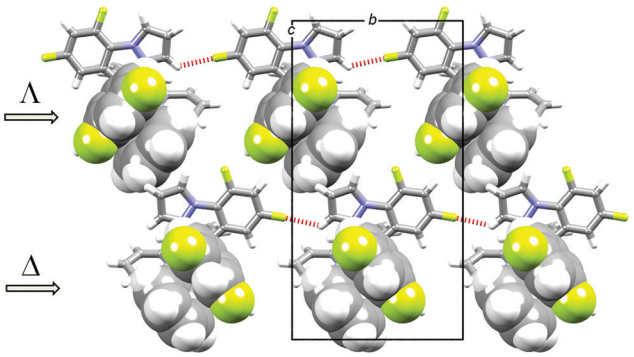

Fig. 5 Association of $[Ir(dfppz)_2(\mathbf{1})]^+$ cations of the same handedness into chains through CH···F hydrogen bonds, and intra-cation face-to-face π-stacking (see text).

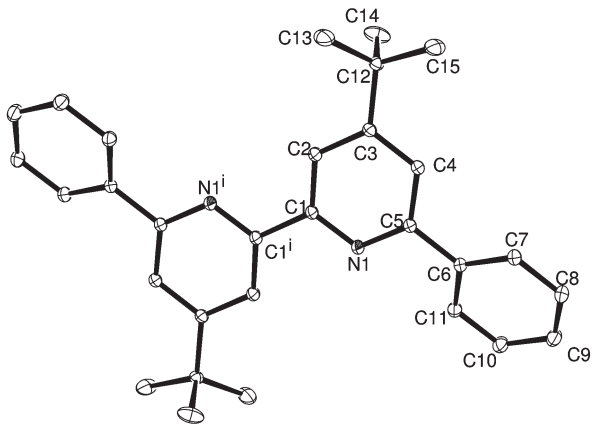

Fig. 6 Structure of compound **3** with ellipsoids plotted at 40% probability level; H atoms omitted. Symmetry code i = $^1/_2 - x$, $^1/_2 - y$, $1 - z$. Selected bond distances: C1–C1^i = 1.4943(10), C1–N1 = 1.3412(7), C5–N1 = 1.3414(7), C5–C6 = 1.4837(7), C3–C12 = 1.5297(7) Å.

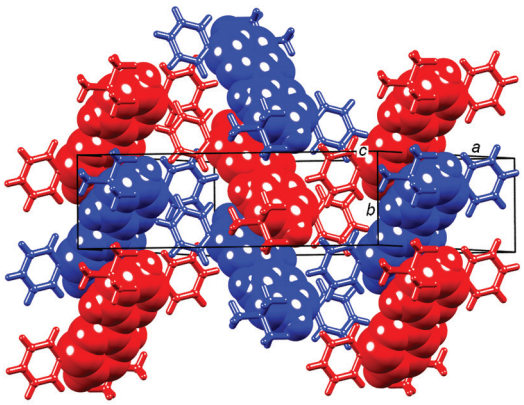

(a)

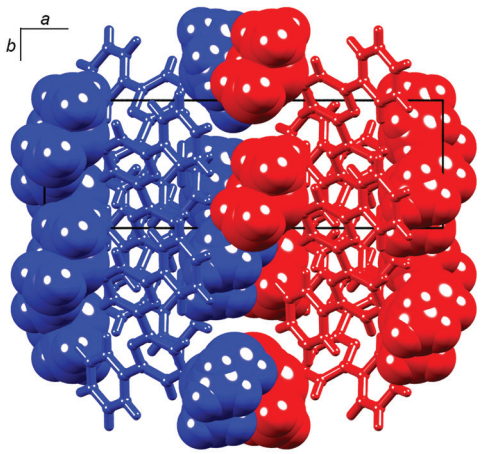

(b)

Fig. 7 Packing of molecules of **3**: (a) with face-to-face π-interactions between pyridine rings highlighted in space-filling representation; (b) a view down the *c*-axis emphasizing the separated domains of ^{t}Bu (space-filling) and aromatic rings (stick representation).

(inter-centroid separation = 3.44 Å) and the angle between their least squares planes is 5.4°, leading to a highly efficient contact. The cations assemble into chains that run parallel to the *b*-axis, the assembly being supported by CH···F hydrogen bonds (C26H26a···F3^i = 2.46 Å, C26···F3^i = 3.142(9) Å, C26–H26a···F3^i = 129°; symmetry code i = x, $1 + y$, z). As Fig. 5 illustrates, cations within the same chain possess the same chirality, while those in adjacent chains are of opposite handedness. The $[PF_6]^-$ anion and CH_2Cl_2 molecule are ordered, and crystal packing is dominated by CH···F_{anion}, CH···F_{ligand}, F···π_{ligand} and Cl···π_{ligand} contacts.

Both **3** and $[Ir(dfppz)_2(\mathbf{3})][PF_6]\cdot CH_2Cl_2$ have been structurally characterized. Although compound **3** has previously been reported,[30,70] its structure has not, to our knowledge, been described. Single crystals of **3** were isolated serendipitously during the synthesis of the complex. Fig. 6 shows that the bpy domain in **3** adopts the expected *trans*-arrangement; bond distances and angles are typical. The molecule is centrosymmetric, and the bpy unit is necessarily planar. The angles between the least squares planes of the phenyl and pyridine rings is 24.6°. Molecules of **3** stack in an offset manner (Fig. 7a), with the pyridine ring containing N1 involved in a face-to-face π-interaction with the ring containing atom N1^{ii} (symmetry code ii = $^1/_2 - x$, $^3/_2 - y$, $1 - z$). Symmetry dictates that the angle between the planes of these rings is 0°; the inter-plane and inter-centroid separations are 3.79 and 3.86 Å, respectively, making these efficient interactions.[69] As Fig. 7a illustrates, the pendant phenyl rings lie in domains in the lattice between the bpy units. A view along the *c*-axis (Fig. 7b) shows that the lattice contains separated domains of ^{t}Bu and aromatic rings.

X-Ray quality crystals of $[Ir(dfppz)_2(\mathbf{3})][PF_6]\cdot CH_2Cl_2$ were grown from a CH_2Cl_2 solution of the complex. The complex crystallizes in the $P2_1/c$ space group with both enantiomers of the $[Ir(dfppz)_2(\mathbf{3})]^+$ cation in the unit cell. The Δ-enantiomer is shown in Fig. 8. The bond parameters in the octahedral coordination sphere of atom Ir1 are, as expected, similar to those of the $[Ir(dfppz)_2(\mathbf{1})]^+$ cation (compare the captions to Fig. 4 and 8). The two $[dfppz]^-$ ligands are essentially planar, but the bpy domain in ligand **3** is twisted with the angle between the planes of the two pyridine rings being 22.0°.

This journal is © The Royal Society of Chemistry 2013

Published on 31 October 2012 on http://pubs.rsc.org | doi:10.1039/C2DT32160B
Downloaded by University of Birmingham on 04 January 2013

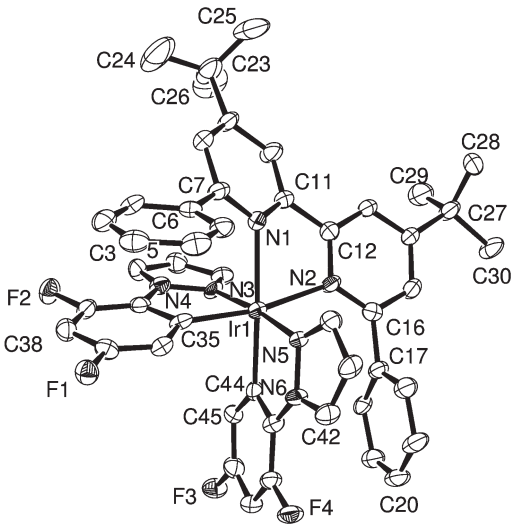

Fig. 8 Structure of the $[Ir(dfppz)_2(\mathbf{3})]^+$ cation in $[Ir(dfppz)_2(\mathbf{3})][PF_6]\cdot CH_2Cl_2$ with ellipsoids plotted at 30% probability level; H atoms omitted. Selected bond parameters: Ir1–N5 = 2.014(10), Ir1–C35 = 2.015(13), Ir1–N3 = 2.029(9), Ir1–C44 = 2.034(12), Ir1–N2 = 2.183(10), Ir1–N1 = 2.221(9), N3–N4 = 1.372(13), N5–N6 = 1.381(12) Å; N2–Ir1–N1 = 76.4(3), C35–Ir1–N3 = 79.8(4), N5–Ir1–C44 = 79.2(4)°.

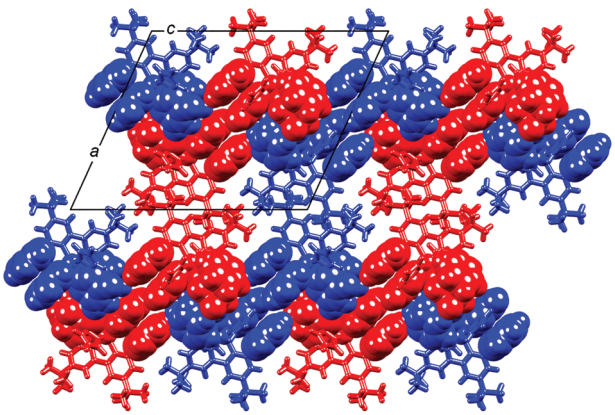

Fig. 9 Packing of $[Ir(dfppz)_2(\mathbf{3})]^+$ cations in $[Ir(dfppz)_2(\mathbf{3})][PF_6]\cdot CH_2Cl_2$. Δ- and Λ-cations are shown in red and blue, respectively, and intra-cation π-stacked domains are shown in space-filling representations.

This is slightly greater than the deformation observed for the same unit in $[Ir(dfppz)_2(\mathbf{1})]^+$. Intra-cation face-to-face π-interactions between a phenyl substituent and an adjacent cyclometallated difluorophenyl ring in $[Ir(dfppz)_2(\mathbf{3})]^+$ are highly efficient; the angles between the least squares planes of rings containing C6/C35 and C17/C44 are 3.7 and 5.0°, respectively, and the inter-centroid distances are 3.46 and 3.47 Å, respectively. A view down the *b*-axis of the unit cell (Fig. 9) illustrates how the Δ- and Λ-cations pack. Cations are arranged with the intra-cation π-stacked domains assembling into sheets parallel to the *bc*-plane, these sheets being separated by sheets of interdigitated ligands **3**. The $[PF_6]^-$ anion and the CH_2Cl_2 molecule are ordered, and CH···F contacts play a dominant role in crystal packing.

Single crystals of $[Ir(dfppz)_2(\mathbf{4})][PF_6]\cdot CH_2Cl_2$ grew from a CH_2Cl_2 solution of the bulk material. The complex crystallizes

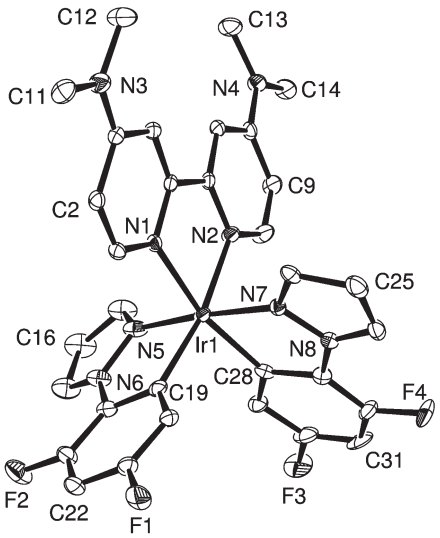

Fig. 10 Structure of the Δ-$[Ir(dfppz)_2(\mathbf{4})]^+$ cation in racemic $[Ir(dfppz)_2(\mathbf{4})][PF_6]\cdot CH_2Cl_2$ with ellipsoids plotted at 30% probability level; H atoms omitted and only the major occupancy sites for the disordered ligand containing atoms N7 and N8 are depicted. Selected bond parameters: Ir1–N1 = 2.109(4), Ir1–N2 = 2.115(5), Ir1–N5 = 1.995(6), Ir1–C28 = 2.009(11), Ir1–N7 = 2.139(9), Ir1–C19 = 2.020(6), C8–N4 = 1.349(7), C3–N3 = 1.343(7), N3–C12 = 1.452(8), N3–C11 = 1.455(8), N4–C13 = 1.448(8), N4–C14 = 1.455(8) Å; N1–Ir1–N2 = 76.20(18), C28–Ir1–N7 = 78.4(5), N5–Ir1–C19 = 80.0(2), C3–N3–C12 = 120.8(5), C3–N3–C11 = 120.1(5), C12–N3–C11 = 118.7(5), C8–N4–C13 = 121.7(5), C8–N4–C14 = 120.0(5), C13–N4–C14 = 117.9(5)°.

in the centrosymmetric space group $P\bar{1}$ with both enantiomers in the unit cell. One of the $[dfppz]^-$ ligands in the $[Ir(dfppz)_2(\mathbf{4})]^+$ cation is disordered and has been modelled over two sites with 66.2 and 33.8% occupancies. Only the major occupancy sites are shown in Fig. 10. Bond parameters within the octahedral environment of the iridium atom are unexceptional (see caption to Fig. 10), as are those in the ligands. Bond angles around atoms N3 and N4 in the NMe_2 groups are consistent with sp^2 hybridization and comparison of the N–C bond lengths involving N3 and N4 (caption to Fig. 10) indicate conjugation of the bpy π-system onto the NMe_2 substituents. The bpy domain is non-planar, with an angle of 15.2° between the planes of the two pyridine rings. This compares with values of 19.5° and 22.0° for coordinated ligands **1** and **3** in $[Ir(dfppz)_2(\mathbf{1})]^+$ and $[Ir(dfppz)_2(\mathbf{3})]^+$, respectively. The trend in values suggests that the presence of the intra-cation π-stacking results in greater twisting of the bpy domain. However, it is interesting to note that even in the absence of these intra-cation interactions, *i.e.* in $[Ir(dfppz)_2(\mathbf{4})]^+$, the bpy unit is also non-planar. In this case, inter-cation interactions appear to be the origin of the deformation. Fig. 11 shows the assembly of Δ- and Λ-$[Ir(dfppz)_2(\mathbf{4})]^+$ cations into chains by interdigitation of $(NMe_2)_2$bpy domains, with each NMe_2 unit lying over a pyridine ring. The $[PF_6]^-$ anion is ordered, and as in the three other complexes described above, $CH\cdots F_{anion}$ and $CH\cdots F_{ligand}$ contacts contribute significantly to crystal packing. The CH_2Cl_2 molecule is disordered and has been modelled over two overlapping sites with fractional occupancies of 63 and 37%.

Published on 31 October 2012 on http://pubs.rsc.org | doi:10.1039/C2DT32160B
Downloaded by University of Birmingham on 04 January 2013

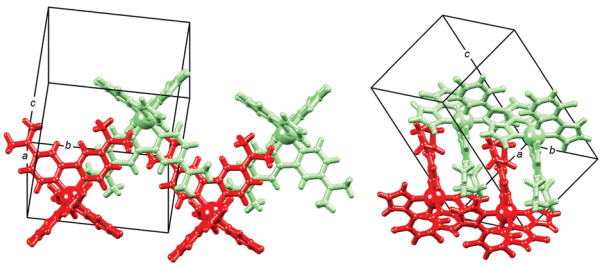

Fig. 11 Two, mutually orthogonal, views of the packing of Δ- (green) and Λ- (red) enantiomers of $[Ir(dfppz)_2(\mathbf{4})]^+$ cations in $[Ir(dfppz)_2(\mathbf{4})][PF_6]\cdot CH_2Cl_2$.

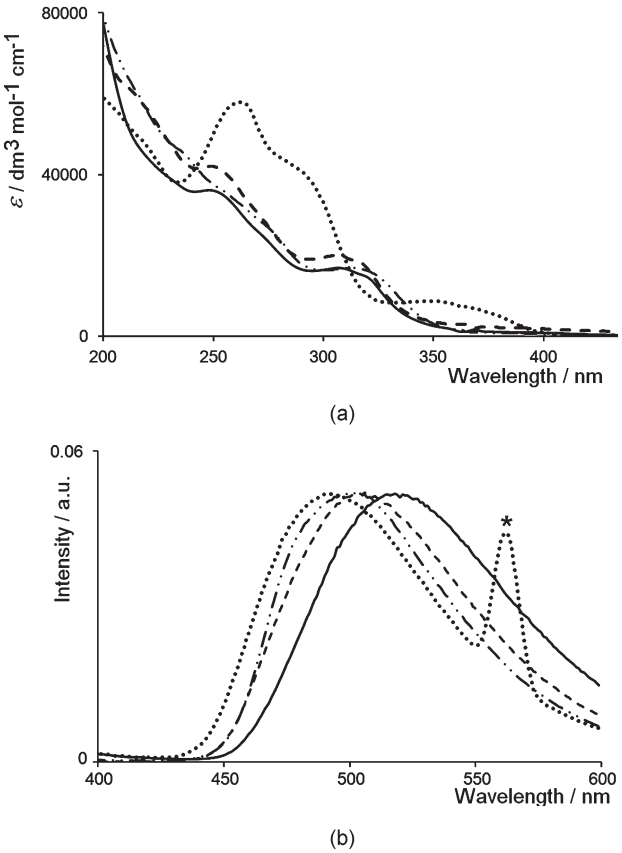

Fig. 12 (a) Electronic absorption spectra of $[Ir(dfppz)_2(N^N)][PF_6]$ (N^N = **1–4**) in MeCN. (b) Normalized emission spectra of $[Ir(dfppz)_2(N^N)][PF_6]$ (N^N = **1–4**) in MeCN; λ_{exc} = 307 nm for N^N = **1**, 307 nm for **2**, 310 nm for **3** and 280 nm for **4** (* = harmonic of excitation). For both (a) and (b): —— N^N = **1**, – – – N^N = **2**, – · · – N^N = **3**, · · · N^N = **4**.

Solution photophysical behaviour of the complexes

The electronic absorption spectra of MeCN solutions of $[Ir(dfppz)_2(N^N)][PF_6]$ (N^N = **1–3**) are similar (Fig. 12a), exhibiting relatively intense bands at 247 and 307 nm for N^N = **1**, 250 and 309 nm for N^N = **2** and 235, 274sh, 306 and 318 nm for N^N = **3**. These absorptions are assigned to ligand-based $\pi^* \leftarrow \pi$ transitions. Enhancement of absorption intensity is observed on going to $[Ir(dfppz)_2(\mathbf{4})][PF_6]$ (λ_{max} = 260, 287 (sh), 352 nm) due to the extension of the bpy π-system onto the NMe_2 substituents in ligand **4**.

The photoluminescence spectra of MeCN solutions of $[Ir(dfppz)_2(N^N)][PF_6]$ (N^N = **1–4**) are shown in Fig. 12b. Excitation between 280 and 310 nm (see caption to Fig. 12b) results in blue emissions with maxima at 517, 505, 501 and 493 nm for N^N = **1**, **2**, **3** and **4**, respectively, with the broad and unstructured shape characteristic of complexes containing a combination of neutral diimine and cyclometallated ligands. The emission maximum for $[Ir(dfppz)_2(\mathbf{1})][PF_6]$ (517 nm) compares with 595 nm for $[Ir(ppy)_2(\mathbf{1})][PF_6]$ (Hppy = 2-phenylpyridine),[71] showing that a change from $[ppy]^-$ to $[dfppz]^-$ as the cyclometallated ligand causes a blue-shift in the emission. Similarly, the emission spectrum is blue-shifted on going from $[Ir(ppy)_2(\mathbf{4})][PF_6]$ (λ_{em} = 520 nm with a shoulder at 491 nm)[72] to $[Ir(dfppz)_2(\mathbf{4})][PF_6]$ (λ_{em} = 493 nm). The effect of going from pyridine to pyrazole in the cyclometallated ligand appears to be negligible, for example, compare λ_{em} = 493 nm with a shoulder at 463 nm for $[Ir(dfppy)_2(\mathbf{4})][PF_6]$[72] (Hdfppy = 2-(2,4-difluorophenyl)-pyridine) with λ_{em} = 493 nm for $[Ir(dfppz)_2(\mathbf{4})][PF_6]$.

Electrochemistry

Each of the $[Ir(dfppz)_2(N^N)][PF_6]$ complexes (N^N = **1–4**) is electrochemically active. Cyclic voltammetric data are presented in Table 3; unless stated otherwise, the electrochemical processes are reversible or near-reversible. The reversible or quasi-reversible oxidation observed for each complex is assigned to an iridium-centred process, while the additional oxidation processes for $[Ir(dfppz)_2(\mathbf{4})][PF_6]$ arise from oxidation of the dimethylamino groups to the radical cations. The metal-centred oxidations occur at similar potentials to that observed for $[Ir(dfppz)_2(N^N)][PF_6]$ (+1.25 V) where N^N = 4,4′-^{t}Bu$_2$bpy,[51] the electron-withdrawing substituents on the C^N ligands shifting the oxidation to more positive potentials when compared to non-fluorinated C^N counterparts.[51] All four complexes exhibit reversible bpy-centred reduction processes; reductions centred on the $[dfppz]^-$ ligand are not observed within the solvent accessible window (to −3 V) as the use of pyrazole induces a significant increase in LUMO energy compared to standard pyridine.[73]

Theoretical calculations

To gain insight into the electronic and optical properties of the complexes $[Ir(dfppz)_2(N^N)][PF_6]$ (N^N = **1–4**), a combined DFT/TD-DFT theoretical investigation was undertaken at the B3LYP/(6-31G**+LANL2DZ) level on the $[Ir(dfppz)_2(N^N)]^+$ cations in the presence of the solvent (acetonitrile) (see the

Table 3 Cyclic voltammetric data with respect to Fc/Fc^+; MeCN solutions with $[^tBu_4N][PF_6]$ supporting electrolyte, and scan rate of 0.1 V s^{-1} (ir = irreversible; qr = quasi-reversible)

Compound	$E_{1/2}^{ox}$/V	$E_{1/2}^{red}$/V	$\Delta E_{1/2}$/V
$[Ir(dfppz)_2(\mathbf{1})][PF_6]$	+1.23	−1.75	2.98
$[Ir(dfppz)_2(\mathbf{2})][PF_6]$	+1.21	−1.83	3.04
$[Ir(dfppz)_2(\mathbf{3})][PF_6]$	$+1.22^{qr}$	−1.85, −2.46	3.07
$[Ir(dfppz)_2(\mathbf{4})][PF_6]$	$+1.04^{qr}$, $+1.47^{ir}$, $+1.57^{ir}$	−2.15	3.19

This journal is © The Royal Society of Chemistry 2013

Published on 31 October 2012 on http://pubs.rsc.org | doi:10.1039/C2DT32160B
Downloaded by University of Birmingham on 04 January 2013

Experimental section for full computational details). The $[Ir(ppy)_2(\mathbf{1})]^+$ cation was also calculated at the same computational level for comparative purposes.

The geometry of the complexes in their ground electronic state (S_0) was fully optimized without imposing any symmetry restriction. Calculations correctly reproduce the near-octahedral coordination of the Ir centre observed in the X-ray structures, and predict geometric parameters in good accord with the experimental data (see Table S1 in the ESI†). For instance, the values computed for the N_{bpy}–Ir–N_{bpy} angle for complexes with N^N = **1** (74.9°), **3** (75.3°) and **4** (75.3°) agree well with the values determined by X-ray diffraction (76.1(2), 76.4(3) and 76.20(18)°, respectively). The values calculated for the N_{dfppz}–Ir–C_{dfppz} angles remain almost constant for the four complexes (average value = 79.6°) in good accord with experiment (79.5°). Calculations also reproduce the intra-cation face-to-face π-stacking of the pendant phenyl substituents of the bpy ligand and the adjacent difluorophenyl ring of one $[dfppz]^-$ ligand. For $[Ir(dfppz)_2(\mathbf{3})]^+$, the calculated inter-centroid distances are 3.69 and 3.70 Å, which slightly overestimate the X-ray values (3.46 and 3.47 Å); this is most likely due to the packing forces acting in the crystal. The bpy domain is predicted to be non-planar with angles of 18.2, 19.9 and 38.3° between the two pyridine planes for the complexes with N^N = **1**, **2** and **3**, respectively, and to be almost planar for $[Ir(dfppz)_2(\mathbf{4})]^+$ (2.4°). These values differ considerably from the values determined by X-ray diffraction for the coordinated ligands **1** (19.5°), **3** (22.0°) and **4** (15.2°) in their respective $[Ir(dfppz)_2(N^N)]^+$ cations revealing the influence of the crystal packing.

Fig. 13 compares the energy and electron density contours calculated for the highest-occupied and the lowest-unoccupied molecular orbitals (HOMO and LUMO, respectively). As already reported for analogous Ir(III) complexes,[51,71,74–76] the HOMO is composed of a mixture of Ir(III) dπ orbitals (t_{2g}) and phenyl π orbitals of the cyclometallated C^N ligands, whereas the LUMO resides on the diimine N^N ligand. Replacement of the $[ppy]^-$ ligand in $[Ir(ppy)_2(\mathbf{1})]^+$ (for which the HOMO is calculated at −5.49 eV) by the more electron-withdrawing $[dfppz]^-$ ligand stabilizes the HOMO of the $[Ir(dfppz)_2(N^N)]^+$ (N^N = **1–3**) cations, for which it is computed to be around −5.80 eV (Fig. 13). This stabilization justifies the anodic shift observed for the first oxidation potential on going from $[Ir(ppy)_2(\mathbf{1})]^+$ (+0.86 V)[12] to $[Ir(dfppz)_2(N^N)]^+$ (N^N = **1–3**) (~+1.20 V, Table 3). The attachment of the electron-donating NMe_2 groups to the bpy ligand in $[Ir(ppy)_2(\mathbf{4})]^+$ destabilizes the HOMO to −5.70 eV and this complex presents a less positive oxidation potential (+1.04 V).

Reduction mainly affects the bpy domain where the LUMO is located (Fig. 13), and this orbital increases in energy along the series N^N = **1** (−2.15 eV), **2** (−2.06 eV), **3** (−2.00 eV) and **4** (−1.63 eV) owing to the introduction of the electron-donating ^{t}Bu groups (**2** and **3**), the increasing twisting of the bpy ligand (**3**) and the attachment of the NMe_2 substituents (**4**). The HOMO–LUMO energy gap therefore increases along the series $[Ir(ppy)_2(\mathbf{1})]^+$ (3.43 eV), $[Ir(dfppz)_2(\mathbf{1})]^+$ (3.68 eV), $[Ir(dfppz)_2(\mathbf{2})]^+$ (3.74 eV), $[Ir(dfppz)_2(\mathbf{3})]^+$ (3.83 eV) and $[Ir(dfppz)_2(\mathbf{4})]^+$ (4.07 eV). This trend supports the increase in the electrochemical gap (2.87,[12] 2.98, 3.04, 3.07 and 3.19 V, respectively) and the blue shift observed in the emission spectra (Fig. 12).

To investigate the nature of the emitting excited state, DFT calculations at the spin-unrestricted UB3LYP level were used for fully optimizing the electronic and molecular structures of the lowest triplet state (T_1) of complexes $[Ir(dfppz)_2(N^N)]^+$ (N^N = **1–4**). Calculations predict that the intra-cation π-stacking is preserved in the T_1 state for complexes with N^N = **1–3**. The main geometrical difference between the electronic ground state S_0 and the excited state T_1 is related to the torsional angle of the bpy ligand that decreases to 11.4, 11.6, 25.1 and 0.8° for complexes with N^N = **1**, **2**, **3** and **4**, respectively.

The T_1 state mainly results from the HOMO → LUMO monoexcitation for complexes with N^N = **1**, **2** and **3** and is computed to lie 2.69, 2.75 and 2.84 eV above S_0 (adiabatic energy differences), respectively. These energies are significantly larger than that calculated for $[Ir(ppy)_2(\mathbf{1})]^+$ (2.40 eV). Excitation to the T_1 state therefore implies an electron transfer from the Ir-dfppz environment to the bpy ligand. This is illustrated in Fig. 14a by the unpaired-electron spin density distribution calculated for $[Ir(dfppz)_2(\mathbf{1})]^+$ (Ir: 0.44e, dfppz: 0.48e, **1**: 1.08e), which perfectly matches the topology of the HOMO → LUMO excitation from which the T_1 state originates.

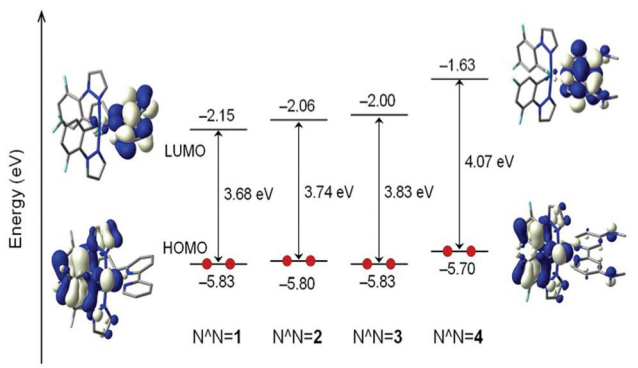

Fig. 13 Schematic diagram showing the electron density contours (0.03 e bohr^{-3}) and the energy values calculated for the HOMO and LUMO of $[Ir(dfppz)_2(N^N)]^+$ (N^N = **1–4**). The HOMO and LUMO of complexes with N^N = **2** and **3** are mostly identical to those displayed for N^N = **1** and **4**.

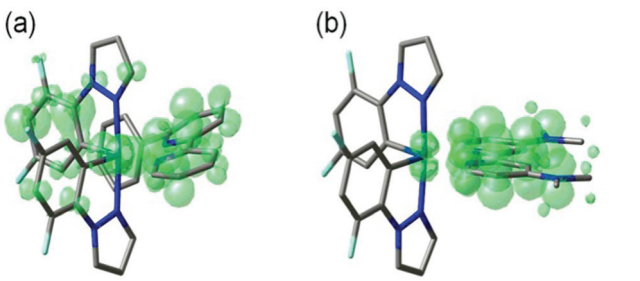

Fig. 14 Spin-density distributions (0.003 e bohr^{-3}) computed for $[Ir(dfppz)_2(N^N)]^+$ complexes with (a) N^N = **1**, and (b) N^N = **4**.

Published on 31 October 2012 on http://pubs.rsc.org | doi:10.1039/C2DT32160B
Downloaded by University of Birmingham on 04 January 2013

The electron transfer associated with the excitation to the T_1 state decreases the twisting of the bpy ligand and causes a small contraction of the coordination sphere of the iridium centre (Table S1†). Calculations therefore suggest that the emitting T_1 state for complexes with N^N = **1**, **2** and **3** has a mixed metal-to-ligand and ligand-to-ligand charge transfer (^{3}MLCT/^{3}LLCT) character in agreement with the broad and unstructured aspect of the emission bands (Fig. 12). This is not however the case for $[Ir(dfppz)_2(\mathbf{4})]^+$, for which, despite the HOMO and LUMO present similar topologies to those calculated for complexes with N^N = **1–3** (Fig. 13), the T_1 state converges to a π–π* ligand-centred (^{3}LC) triplet of the 4,4′-dimethylamino-2,2′-bipyridine ligand with a small contribution from the metal (0.11e) (Fig. 14b). The difference for $[Ir(dfppz)_2(\mathbf{4})]^+$ is that in this complex, the HOMO − 1 and HOMO − 2 correspond to almost degenerate combinations of Ir-(t_{2g}) and π orbitals of the ancillary ligand and lie very close in energy (−5.75 eV) to the HOMO (−5.70 eV) (see Fig. S1†). As a consequence, the HOMO − 2 → LUMO and HOMO − 1 → LUMO excitations give rise to ^{3}LC states lower in energy than the HOMO → LUMO excitation (see TD-DFT results in Table S2†) and the emitting T_1 state has a predominant ^{3}LC character.

To estimate the phosphorescence emission energy, the vertical energy difference between T_1 and S_0 was computed by performing a single-point calculation of S_0 at the optimized minimum-energy geometry of T_1. Calculations lead to vertical emission energies of 2.39 (519), 2.45 (506), 2.42 (511) and 2.54 eV (488 nm) for complexes with N^N = **1**, **2**, **3** and **4**, respectively, in good agreement with the experimental emission maxima (517, 505, 501 and 493 nm, respectively).

Thin-film photophysical behaviour of the complexes

The photophysics of complexes $[Ir(dfppz)_2(N^N)][PF_6]$ (N^N = **1–4**) was also studied in thin-film (5% in weight of the complex in PMMA). The thin-film photoluminescence spectra were characterized by maxima at 493, 492, 493 and 489 nm with quantum yields of 100%, 99%, 60% and 89% for N^N = **1**, **2**, **3** and **4**, respectively, when excited with a wavelength of 310 nm (Fig. 15). These quantum yields make the complexes amongst the most efficient ionic iridium emitters, and are in line with those previously reported for iridium(III) complexes bearing difluorophenylpyridine cyclometallating ligands together with a neutral diimine ligand incorporating bulky groups.[72]

Photoluminescence of the complexes mixed with the ionic liquid (IL) 1-butyl-3-methylimidazolium hexafluoridophosphate $[BMIM^+ : PF_6^-]$ in a 4 to 1 molar ratio were also characterized resulting in peak maxima of 510, 500, 504 and 510 nm with quantum yields of 89%, 66%, 15% and 45% for N^N = **1**, **2**, **3** and **4**, respectively. The slight red-shift that is observed in the emission of the complexes mixed with the IL compared with the diluted thin films in PMMA can be attributed to concentration effects. The lower quantum yield is due to the higher concentration of complex in the film that promotes the self-quenching between molecules of the complex. However, the quantum yield remains high probably because the bulky groups on the ancillary ligand of the complexes make the exciton diffusion by energy transfer between adjacent molecules more difficult. The complex with N^N = **3** exhibits lower quantum yields when compared with those containing N^N = **1**, **2** and **4**. A possible explanation to this behaviour is that the presence of the second pendant phenyl substituent increases the possibility for a non-radiative decay to the ground state due to the closer proximity of metal-centred ^{3}MC states to the T_1 emitting state, as was previously shown both experimentally and theoretically for a family of analogous $[Ir(ppy)_2(N^N)][PF_6]$ complexes.[77,78]

Electroluminescence

To study the electroluminescent behaviour of the complexes $[Ir(dfppz)_2(N^N)][PF_6]$ (N^N = **1–4**), LEC devices were prepared by spin-coating a 90 nm layer of PEDOT : PSS on top of a patterned indium tin oxide (ITO)-coated glass substrate followed by an 90 nm active layer consisting of complex and the [BMIM]-$[PF_6]$ ionic liquid at a molar ratio of 4 to 1. The IL is added to reduce the turn-on time. A 70 nm aluminium layer was thermally evaporated as the top electrode contact.

The electroluminescent spectra of LEC devices incorporating $[Ir(dfppz)_2(N^N)][PF_6]$ (N^N = **1–4**) complexes are shown in Fig. 16. Complexes with N^N = **1** and **2** have emission maxima

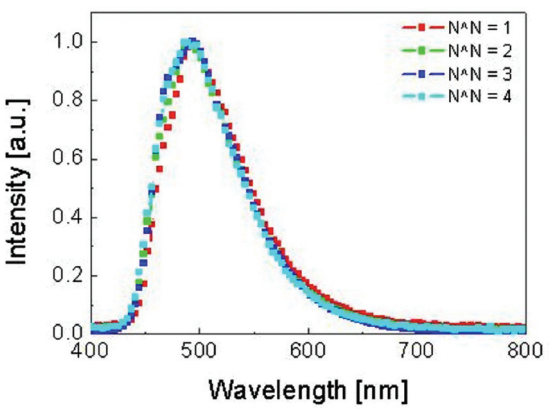

Fig. 15 Photoluminescence spectra of $[Ir(dfppz)_2(N^N)][PF_6]$ (N^N = **1–4**) in thin films of 5% in weight in PMMA.

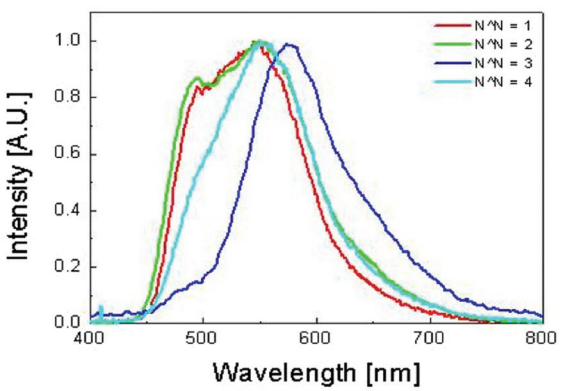

Fig. 16 Electroluminescence spectra of ITO/PEDOT : PSS/$[Ir(dfppz)_2$-$(N^N)]$-$[PF_6]$: [BMIM][PF_6](4 : 1)/Al devices.

This journal is © The Royal Society of Chemistry 2013

Published on 31 October 2012 on http://pubs.rsc.org | doi:10.1039/C2DT32160B
Downloaded by University of Birmingham on 04 January 2013

Table 4 Performance of LEC devices biased with a 50% duty cycle pulsed current block wave at a frequency of 1000 Hz at an average current density of 100 A m^{-2}

$[Ir(dfppz)_2(N^N)][PF_6]$	t_{on}	L_{max}/cd m^{-2}	$t_{1/2}$/h	Efficacy/cd A^{-1}	Power efficiency/lm W^{-1}	EQE/%
N^N = **1**	3.8 h	52	12.2	0.5	0.25	0.16
N^N = **2**	<5 s	572	0.02	5.2	1.82	1.81
N^N = **3**	0.4 h	205	4.4	2.0	0.91	0.70
N^N = **4**	<5 s	67	0.01	0.5	0.18	0.16

at 545 and 550 nm with a second peak at 494 and 492 nm, respectively. Complexes with N^N = **3** and **4** show only one emission maximum peaking at 574 and 551 nm, respectively. The CIE coordinates are (0.33, 0.53), (0.33, 0.50), (0.48, 0.50) and (0.37, 0.53) for N^N = **1**, **2**, **3** and **4**, respectively. The strong red-shift observed on the electroluminescence emission compared to the photoluminescence emission is frequently observed in LECs using wide bandgap emitters. The origin of this effect is not completely clear, but has been attributed to morphological effects and also to light-out coupling effects.[75]

To determine the device performances, LEC devices were operated by a pulsed current driving using a 50% duty cycle block-wave at 1000 Hz and a current density (averaged over the on- and off-pulse time) of 100 A m^{-2}. The results are summarized in Table 4. The devices show maximum luminances of 52, 572, 205 and 67 cd m^{-2} with lifetimes (time to reach half of the maximum luminance) of 12.2, 0.02, 4.4 and 0.01 hours for N^N = **1**, **2**, **3** and **4**, respectively. Their efficacies are 0.5, 5.2, 2.0 and 0.5 cd A^{-1} and their power efficiencies 0.25, 1.82, 0.91 and 0.18 lm W^{-1} for N^N = **1**, **2**, **3** and **4**, respectively. The poor performance of N^N = **4** can be attributed to the possible protonation of the amine groups attached to the neutral diimine ligand due to the migration of protons from the PEDOT : PSS layer to the active layer.

Conclusions

We have reported the synthesis and characterization of four complexes of type $[Ir(dfppz)_2(N^N)][PF_6]$ (N^N = **1–4**) in order to investigate the effects of combining electron-withdrawing substituents in the cyclometallated $[dfppz]^-$ ligand with electron-releasing ^{t}Bu or NMe_2 substituents in the ancillary bpy ligand. The substituents are designed to shift the emission maxima of the complexes towards the blue. Structural determinations of ligand **3**, the precursor $[Ir_2(dfppz)_4(\mu\text{-}Cl)_2]\cdot CH_2Cl_2$ and the complexes $4\{[Ir(dfppz)_2(\mathbf{1})][PF_6]\}\cdot 3CH_2Cl_2$, $[Ir(dfppz)_2(\mathbf{3})][PF_6]\cdot CH_2Cl_2$ and $[Ir(dfppz)_2(\mathbf{4})][PF_6]\cdot CH_2Cl_2$ confirm that intermolecular face-to-face π-stacking and intra-cation stacking in the complexes are dominant packing interactions. The latter involve the phenyl substituents in the $[Ir(dfppz)_2(N^N)]^+$ (N^N = **1–3**) cations, and in solution, rotation of the phenyl groups in coordinated ligands **1**, **2** or **3** is hindered. The four complexes are blue emitters in solution (λ_{em} = 517, 505, 501 and 493 nm for N^N = **1**, **2**, **3** and **4**). The redox behaviours of $[Ir(dfppz)_2(N^N)][PF_6]$ (N^N = **1–3**) are similar, and the introduction of the electron-releasing NMe_2 substituents onto the N^N ligand shifts the metal-centred oxidation to less positive potentials. Theoretical calculations reveal that the intra-cation π-stacking is preserved in the emitting triplet state of the $[Ir(dfppz)_2(N^N)]^+$ (N^N = **1–3**) cations that shows a mixed ^{3}MLCT/^{3}LLCT character in agreement with the broad and unstructured aspect of the emission bands. The NMe_2 substituents enlarge the HOMO–LUMO gap and blue-shifts the emission of $[Ir(dfppz)_2(\mathbf{4})]^+$. All the complexes can be used to generate electroluminescent devices without additional additives such as charge transporting molecules. The electroluminescence spectra of the LECs using these complexes is slightly red-shifted with respect to the photoluminescence spectra. This is an interesting phenomena that need to be investigated further.

Acknowledgements

We acknowledge the Swiss National Science Foundation, the University of Basel, the Swiss Nanoscience Institute, the National Centre of Competence in Research "Nanoscale Science", the Spanish Ministry of Economy and Competitiveness (MINECO) (MAT2011-24594, CTQ2009-08790 and Consolider-Ingenio CSD2007-00010), the Generalitat Valenciana (PROMETEO/2012/053), the European Union (CELLO, STRP 248043; https://www.cello-project.eu/) and the European Research Council (Advanced Grant 267816 LiLo) for financial support. D.T. and M.D. acknowledge the support of a FPU grant of the Spanish Ministry of Education, Culture and Sport (MECD). Dr Stefan Graber is thanked for the synthesis of ligands **2** and **3**. Dr Peter Kopecky is thanked for recording some of the ^{1}H NMR spectra.

Notes and references

1 L. He, L. Duan, J. Qiao, D. Zhang, L. Wang and Y. Qiu, *Appl. Phys. A*, 2010, **100**, 1035.
2 R. D. Costa, E. Ortí, H. J. Bolink, F. Monti, G. Accorsi and N. Armaroli, *Angew. Chem., Int. Ed.*, 2012, **51**, 8178.
3 K. Walzer, B. Maennig, M. Pfeiffer and K. Leo, *Chem. Rev.*, 2007, **107**, 1233.
4 Q. Pei, G. Yu, C. Zhang, Y. Yang and A. J. Heeger, *Science*, 1995, **269**, 1086.
5 C. H. Lyons, E. D. Abbas, J. K. Lee and M. F. Rubner, *J. Am. Chem. Soc.*, 1998, **120**, 12100.
6 F. G. Gao and A. J. Bard, *J. Am. Chem. Soc.*, 2000, **122**, 7426.
7 J. D. Slinker, J. Rivnay, J. S. Moskowitz, J. B. Parker, S. Bernhard, H. D. Abruña and G. G. Malliaras, *J. Mater. Chem.*, 2007, **17**, 2976.

Published on 31 October 2012 on http://pubs.rsc.org | doi:10.1039/C2DT32160B
Downloaded by University of Birmingham on 04 January 2013

8 J. C. deMello, N. Tessler, S. C. Graham and R. H. Friend, *Phys. Rev. B: Condens. Matter*, 1998, **57**, 12951.
9 J. D. Slinker, J. A. DeFranco, M. J. Jaquith, W. R. Silveira, Y. Zhong, J. M. Moran-Mirabal, H. G. Graighead, H. D. Abruña, J. A. Marohn and G. G. Malliaras, *Nat. Mater.*, 2007, **6**, 894.
10 S. Graber, K. Doyle, M. Neuburger, C. E. Housecroft, E. C. Constable, R. D. Costa, E. Ortí, D. Repetto and H. J. Bolink, *J. Am. Chem. Soc.*, 2008, **130**, 14944.
11 H. C. Su, H. F. Chen, F. C. Fang, C. C. Liu, C. C. Wu, K. T. Wong, Y. H. Liu and S. M. Peng, *J. Am. Chem. Soc.*, 2008, **130**, 3413.
12 R. D. Costa, E. Ortí, H. J. Bolink, S. Graber, C. E. Housecroft and E. C. Constable, *J. Am. Chem. Soc.*, 2010, **132**, 5978.
13 T. Hu, L. He, L. Duan and Y. Qiu, *J. Mater. Chem.*, 2012, **22**, 4206.
14 D. Tordera, S. Meier, M. Lenes, R. D. Costa, E. Ortí, W. Sarfert and H. J. Bolink, *Adv. Mater.*, 2012, **24**, 897.
15 D. Tordera, M. Delgado, E. Ortí, H. J. Bolink, J. Frey, Md. K. Nazeeruddin and E. Baranoff, *Chem. Mater.*, 2012, **24**, 1896.
16 M. Lenes, G. García-Belmonte, D. Tordera, A. Pertegás, J. Bisquert and H. J. Bolink, *Adv. Funct. Mater.*, 2011, **21**, 1581.
17 P. Matyba, K. Maturova, M. Kemerink, N. D. Robinson and L. Edman, *Nat. Mater.*, 2009, **8**, 672.
18 D. B. Rodovsky, O. G. Reid, L. S. C. Pingree and D. S. Ginger, *ACS Nano*, 2010, **4**, 2673.
19 S. van Reenen, P. Matyba, A. Dzwilewski, R. A. J. Janssen, L. Edman and M. Kemerink, *J. Am. Chem. Soc.*, 2010, **132**, 13776.
20 L. He, L. Duan, J. Qiao, R. Wang, P. Wei, L. Wang and Y. Qiu, *Adv. Funct. Mater.*, 2008, **18**, 2123.
21 L. He, L. Duan, J. Qiao, D. Zhang, L. Wang and Y. Qiu, *Chem. Commun.*, 2011, **47**, 6467.
22 L. He, J. Qiao, L. Duan, G. Dong, D. Zhang, L. Wang and Y. Qiu, *Adv. Funct. Mater.*, 2009, **19**, 2950.
23 B. Chen, Y. Li, W. Yang, W. Luo and H. Wu, *Org. Electron.*, 2011, **12**, 766.
24 M. Mydlak, C. Bizzarri, D. Hartmann, W. Sarfert, G. Schmid and L. De Cola, *Adv. Funct. Mater.*, 2010, **20**, 1812.
25 C.-H. Yang, J. Beltran, V. Lemaur, J. Cornil, D. Hartmann, W. Sarfert, R. Frohlich, C. Bizzarri and L. De Cola, *Inorg. Chem.*, 2010, **49**, 9891.
26 L. He, L. Duan, J. Qiao, G. Dong, L. Wang and Y. Qiu, *Chem. Mater.*, 2010, **22**, 3535.
27 M. Nonoyama, *Bull. Chem. Soc. Jpn.*, 1974, **47**, 767.
28 E. C. Constable, R. P. G. Henney, T. A. Leese and D. A. Tocher, *J. Chem. Soc., Dalton Trans.*, 1990, 443.
29 W. Lu, B.-X. Mi, M. C. W. Chan, Z. Hui, C.-M. Che, N. Zu and S.-T. Lee, *J. Am. Chem. Soc.*, 2004, **126**, 4958.
30 M. Lepeltier, T. K.-M. Lee, K. K.-W. Lo, L. Toupet, H. Le Bozec and V. Guerchais, *Eur. J. Inorg. Chem.*, 2005, 110.
31 D. Zhang, J. P. Telo, C. Liao, S. E. Hightower and E. L. Clennan, *J. Phys. Chem. A*, 2007, **111**, 13567.
32 *APEX2, version 2 User Manual, M86-E01078*, Bruker Analytical X-ray Systems, Inc., Madison, WI, 2006.
33 A. Altomare, G. Cascarano, G. Giacovazzo, A. Guagliardi, M. C. Burla, G. Polidori and M. Camalli, *J. Appl. Crystallogr.*, 1994, **27**, 435.
34 P. W. Betteridge, J. R. Carruthers, R. I. Cooper, K. Prout and D. J. Watkin, *J. Appl. Crystallogr.*, 2003, **36**, 1487.
35 Stoe & Cie, *IPDS software v 1.26*, Stoe & Cie, Darmstadt, Germany, 1996.
36 G. M. Sheldrick, *Acta Crystallogr., Sect. A: Fundum. Crystallogr.*, 2008, **64**, 112.
37 L. J. Farrugia, *J. Appl. Crystallogr.*, 1997, **30**, 565.
38 I. J. Bruno, J. C. Cole, P. R. Edgington, M. K. Kessler, C. F. Macrae, P. McCabe, J. Pearson and R. Taylor, *Acta Crystallogr., Sect. B: Struct. Sci.*, 2002, **58**, 389.
39 C. F. Macrae, I. J. Bruno, J. A. Chisholm, P. R. Edgington, P. McCabe, E. Pidcock, L. Rodriguez-Monge, R. Taylor, J. van de Streek and P. A. Wood, *J. Appl. Crystallogr.*, 2008, **41**, 466.
40 M. J. Frisch, G. W. Trucks, H. B. Schlegel, G. E. Scuseria, M. A. Robb, J. R. Cheeseman, G. Scalmani, V. Barone, B. Mennucci, G. A. Petersson, H. Nakatsuji, M. Caricato, X. Li, H. P. Hratchian, A. F. Izmaylov, J. Bloino, G. Zheng, J. L. Sonnenberg, M. Hada, M. Ehara, K. Toyota, R. Fukuda, J. Hasegawa, M. Ishida, T. Nakajima, Y. Honda, O. Kitao, H. Nakai, T. Vreven, J. Montgomery Jr., J. E. Peralta, F. Ogliaro, M. Bearpark, J. J. Heyd, E. Brothers, K. N. Kudin, V. N. Staroverov, T. Keith, R. Kobayashi, J. Normand, K. Raghavachari, A. Rendell, J. C. Burant, S. S. Iyengar, J. Tomasi, M. Cossi, N. Rega, J. M. Millam, M. Klene, J. E. Knox, J. B. Cross, V. Bakken, C. Adamo, J. Jaramillo, R. Gomperts, R. E. Stratmann, O. Yazyev, A. J. Austin, R. Cammi, C. Pomelli, J. W. Ochterski, R. L. Martin, K. Morokuma, V. G. Zakrzewski, G. A. Voth, P. Salvador, J. J. Dannenberg, S. Dapprich, A. D. Daniels, Ö. Farkas, J. B. Foresman, J. V. Ortiz, J. Cioslowski and D. J. Fox, *GAUSSIAN 09 (Revision C.01)*, Gaussian, Inc., Wallingford, CT, 2010.
41 A. D. Becke, *J. Chem. Phys.*, 1993, **98**, 5648.
42 C. Lee, W. Yang and R. G. Parr, *Phys. Rev. B: Condens. Matter*, 1988, **37**, 785.
43 M. M. Francl, W. J. Pietro, W. J. Hehre, J. S. Binkley, M. S. Gordon, D. J. Defrees and J. A. Pople, *J. Chem. Phys.*, 1982, **77**, 3654.
44 P. J. Hay and W. R. Wadt, *J. Chem. Phys.*, 1985, **82**, 299.
45 J. Tomasi and M. Persico, *Chem. Rev.*, 1994, **94**, 2027.
46 C. S. Cramer and D. G. Truhlar, *Solvent Effects and Chemical Reactivity*, Kluwer, Dordrecht, 1996, pp. 1–80.
47 J. Tomasi, B. Mennucci and R. Cammi, *Chem. Rev.*, 2005, **105**, 2999.
48 A. V. Marenich, C. J. Cramer and D. G. Truhlar, *J. Phys. Chem. B*, 2009, **113**, 6378.
49 See for example: F. Neve, A. Crispini, S. Campagna and S. Serroni, *Inorg. Chem.*, 1999, **38**, 2250 and references cited therein.
50 A. B. Tamayo, B. D. Alleyne, P. I. Djurovich, S. Lamansky, I. Tsyba, N. N. Ho, R. Bau and M. E. Thompson, *J. Am. Chem. Soc.*, 2003, **125**, 7377.

 This journal is © The Royal Society of Chemistry 2013

Published on 31 October 2012 on http://pubs.rsc.org | doi:10.1039/C2DT32160B
Downloaded by University of Birmingham on 04 January 2013

51 A. B. Tamayo, S. Garon, T. Sajoto, P. I. Djurovich, I. M. Tsyba, R. Bau and M. E. Thompson, *Inorg. Chem.*, 2005, **44**, 8723.
52 C.-H. Yang, S.-W. Li, Y. Chi, Y.-M. Cheng, Y.-S. Yeh, P.-T. Chou, G.-H. Lee, C.-H. Wang and C.-F. Shu, *Inorg. Chem.*, 2005, **44**, 7770.
53 K. Dedeian, J. Shi, N. Shepherd, E. Forsythe and D. C. Moron, *Inorg. Chem.*, 2005, **44**, 4445.
54 C.-J. Chang, C.-H. Yang, K. Chen, Y. Chi, C.-F. Shu, M.-L. Ho, Y.-S. Yeh and P.-T. Chou, *Dalton Trans.*, 2007, 1881.
55 N. M. Shavaleev, R. Scopelliti, E. Baranoff, M. Grätzel and Md. K. Nazeeruddin, *Inorg. Chim. Acta*, 2012, **383**, 316.
56 G.-G. Shan, H.-B. Li, Z.-C. Mu, D.-X. Zhu, Z.-M. Su and Y. Liao, *J. Organomet. Chem.*, 2012, **702**, 27.
57 G.-G. Shan, H.-B. Li, H.-T. Cao, D.-X. Zhu, P. Li, Z.-M. Su and Y. Liao, *Chem. Commun.*, 2012, **48**, 2000.
58 F. O. Garces, K. Dedeian, N. L. Keder and R. J. Watts, *Acta Crystallogr., Sect. C: Cryst. Struct. Commun.*, 1993, **49**, 1117.
59 S. Bettington, A. L. Thompson, A. Beeby and A. E. Goeta, *Acta Crystallogr., Sect. E: Struct. Rep. Online*, 2004, **60**, m827.
60 L.-Q. Chen, C.-L. Yang and J.-G. Qin, *Acta Crystallogr., Sect. C: Cryst. Struct. Commun.*, 2005, **61**, m513.
61 S. Bettington, M. Tavasli, M. R. Bryce, A. S. Batsanov, A. L. Thompson, H. A. Al Attar, F. B. Dias and A. P. Monkman, *J. Mater. Chem.*, 2006, **16**, 1046.
62 V. V. Krisyuk, A. E. Turgambaeva, J. Lee and S.-W. Rhee, *Trans. Met. Chem.*, 2005, **30**, 786.
63 K. A. McGee and K. R. Mann, *Inorg. Chem.*, 2007, **46**, 7800.
64 M. Graf, M. Thesen, H. Kruger, P. Mayer and K. Sunkel, *Inorg. Chem. Commun.*, 2009, **12**, 701.
65 L. Norel, M. Rudolph, N. Vanthuyne, J. A. G. Williams, C. Lescop, C. Roussel, J. Autschbach, J. Crassous and R. Reau, *Angew. Chem., Int. Ed.*, 2010, **49**, 99.
66 D. L. Davies, M. P. Lowe, K. S. Ryder, K. Singh and S. Singh, *Dalton Trans.*, 2011, **40**, 1028.
67 Z.-Q. Wang, C. Xu, X.-M. Dong, Y.-P. Zhang, X.-Q. Hao, J.-F. Gong, M.-P. Song and B.-M. Ji, *Inorg. Chem. Commun.*, 2011, **14**, 316.
68 E. Andreiadis, D. Imbert, J. Pecaut, A. Calborean, I. Ciofini, C. Adamo, R. Demadrille and M. Mazzanti, *Inorg. Chem.*, 2011, **50**, 8197.
69 C. Janiak, *J. Chem. Soc., Dalton Trans.*, 2000, 3885.
70 T. Ben Hadda, I. Zidane, S. A. Moyaamd and H. Le Bozec, *Polyhedron*, 1996, **15**, 1571.
71 R. D. Costa, E. Ortí, H. J. Bolink, S. Graber, C. E. Housecroft and E. C. Constable, *Adv. Funct. Mater.*, 2010, **20**, 1511.
72 F. De Angelis, S. Fantacci, N. Evans, C. Klein, S. M. Zakeeruddin, J.-E. Moser, K. Kalyanasundaram, H. J. Bolink, M. Grätzel and M. K. Nazeeruddin, *Inorg. Chem.*, 2007, **46**, 5989.
73 T. Sajoto, P. I. Djurovich, A. Tamayo, M. Yousufuddin, R. Bau and M. E. Thompson, *Inorg. Chem.*, 2005, **44**, 7992.
74 M. S. Lowry, W. R. Hudson, R. A. Pascal and S. Bernhard, *J. Am. Chem. Soc.*, 2004, **126**, 14129.
75 H. J. Bolink, L. Cappelli, S. Cheylan, E. Coronado, R. D. Costa, N. Lardiés, M. K. Nazeeruddin and E. Ortí, *J. Mater. Chem.*, 2007, **17**, 5032.
76 R. D. Costa, E. Ortí, H. J. Bolink, S. Graber, S. Schaffner, M. Neuburger, C. E. Housecroft and E. C. Constable, *Adv. Funct. Mater.*, 2009, **19**, 3456.
77 R. D. Costa, E. Ortí, H. J. Bolink, S. Graber, C. E. Housecroft, M. Neuburger, S. Schaffner and E. C. Constable, *Chem. Commun.*, 2009, 2029.
78 R. D. Costa, F. Monti, G. Accorsi, A. Barbieri, H. J. Bolink, E. Ortí and N. Armaroli, *Inorg. Chem.*, 2011, **50**, 7229.